PHYSICS OF FLUIDS **24**, 127101 (2012)

Explicit invariant manifolds and specialised trajectories in a class of unsteady flows

Sanjeeva Balasuriya[a)]
Department of Mathematics, Connecticut College, New London, Connecticut 06320, USA and School of Mathematical Sciences, University of Adelaide, SA 5005, Australia

(Received 10 January 2012; accepted 6 November 2012; published online 11 December 2012)

A class of unsteady two- and three-dimensional velocity fields for which the associated stable and unstable manifolds of the Lagrangian trajectories are explicitly known is introduced. These invariant manifolds form the important time-varying flow barriers which demarcate coherent fluids structures, and are associated with hyperbolic trajectories. Explicit expressions are provided for time-evolving hyperbolic trajectories (the unsteady analogue of saddle stagnation points), which are proven to be hyperbolic in the sense of exponential dichotomies. Elliptic trajectories (the unsteady analogue of stagnation points around which there is rotation, i.e., the "centre of a vortex") are similarly explicitly expressed. While this class of models possesses integrable Lagrangian motion since formed by applying time-dependent spatially invertible transformations to steady flows, their hyperbolic/elliptic trajectories can be made to follow any user-specified path. The models are exemplified through two classical flows: the two-dimensional two-gyre Duffing flow and the three-dimensional Hill's spherical vortex. Extensions of the models to finite-time and nonhyperbolic manifolds are also presented. Given the paucity of explicit unsteady examples available, these models are expected to be useful testbeds for researchers developing and improving diagnostic methods for tracking flow structures in genuinely time-dependent flows.
 [http://dx.doi.org/10.1063/1.4769979]

I. INTRODUCTION

Characterising transport barriers and fluid blobs that move as coherent entities continues to be an intensive area of study, with many applications in oceanography and atmospheric science. These govern the transport of key quantities such as potential vorticity, heat, salinity, bio-organisms and pollutants, and consequently are significant in our environment and climate.[1–9] Understanding and controlling such transport barriers and coherent structures is also one way of attempting to increase mixing properties in microfluidic devices.[10–13]

Defining important flow barriers is easy in two-dimensional steady laminar flows, in which the flow separators which demarcate regions of disparate fluid motion are invariant (stable and unstable) manifolds of stagnation points. Extending these definitions to time-periodic two-dimensional flows is well established;[14] the manifolds are associated with the Poincaré map which strobes the flow at time intervals equal to the periodicity of the flow. There is some understanding on the notion of invariant manifolds when permitting time-aperiodicity[15–19] and three-dimensionality,[20–23] but some difficulties remain. Under general time-dependent (unsteady) flow, the entities analogous to saddle stagnation points are "hyperbolic trajectories." For example, if viewing a steady flow with a saddle stagnation point from a boat travelling at a constant speed, the flow would have trivial unsteadiness, and the entity corresponding to the original stagnation point would be a specialised trajectory which travels at a constant speed, which therefore *cannot* be obtained by seeking points at which the fluid is instantaneously at rest. It is the time-varying stable and unstable manifolds of

a)sanjeevabalasuriya@yahoo.com.

this hyperbolic trajectory which form the crucial flow barriers. While the analysis of instantaneous stagnation points is useful in many applications, such as groundwater modelling,[24,25] macro- and micro-mixing devices,[26–31] and oceanographic flows,[5,32–36] this example shows that such entities have no meaning in determining important flow regulators in *unsteady* flows, except in certain limiting situations such as when the structures are moving sufficiently slowly.[37,38] Thus hyperbolic trajectories need to be determined, along with their invariant manifolds, but their definition is based on "exponential dichotomies,"[39,40] in which the flow is linearised along the purported hyperbolic trajectory, and the idea is to check whether there is a splitting into directions in which exponential expansion and contraction occur. In the unsteady situation exponential dichotomies *cannot* be imputed based on frozen-time eigenvalues of the linearisation matrix, and hence this definition is extremely difficult to use to identify hyperbolic trajectories even when the unsteady velocity is explicitly known. Three-dimensional flows, even in the steady situation, offer additional challenges, since the stable and unstable manifolds can be associated with periodic orbits (which require computational effort to determine in contrast to stagnation points), and both one- and two-dimensional invariant manifolds are generically present.

Even under idealised steady conditions, computing global invariant manifolds is difficult, and usually requires clever algorithms.[41] In *real* unsteady flows—either observational, experimental or numerical—computing such flow barriers becomes prohibitive. Data from such flows are typically noisy, discrete in space and time, and also limited to finite times. This last issue causes immediate problems because hyperbolic trajectories, and stable and unstable manifolds, require *infinite-time* velocity fields in order to quantify exponential decays. Therefore, a variety of *finite-time* tools for characterising flow barriers and transport have emerged, of which finite-time Lagrangian coherent structures (LCSs) now play a major role. Their definition[20,42] is associated with material surfaces which have locally maximal attracting or repelling properties, and are equally legitimate in the unsteady setting. Nevertheless, computing LCSs (or alternative entities which are associated with flow barriers) remains a challenging task, for which a variety of diagnostic methods has been developed.[41,43–45] Ridges of finite-time Lyapunov exponent (FTLE) fields are one such diagnostic which has increasing popularity across many fluids-related disciplines,[3–5,46–50] and continues to be developed.[51–54] While FTLEs can give false positives or negatives for LCSs,[55–58] it is possible to establish their accuracy under certain conditions.[55,59] Another class of diagnostics is associated with averages along trajectories,[60–64] while yet another deals with Perron-Frobenius (transfer) and Koopman operators.[61,65–70] There are also a variety of very recently developed methods[71–74] which are seemingly unrelated to better established methods or to one another. Each diagnostic method has its challenges associated with computational complexity and data requirements, and at the basic level whether the method reliably and unequivocally identifies LCSs; hence the continuing interest in developing and refining such diagnostic methods.

Another important aspect which has received less attention (possibly because of the difficulties in conceptualising these effects both theoretically and diagnostically) is the potential for there to be a trajectory which is *nonhyperbolic* in the sense of exponential decays, but which nevertheless has attached to it stable and unstable manifolds which form crucial flow separators. The analogous situation in steady flows would be nonhyperbolic fixed points whose nearby phase space behaviour "looks like" saddle points, even though the rates of decay are not exponential. An example is the system $\dot{x} = -x^3$, $\dot{y} = y^3$, for which the stagnation point $(0, 0)$ is not hyperbolic, since all derivatives of the velocity field are zero at this point. Technically speaking, there is now a two-dimensional centre manifold[75] and in such situations linearisation fails to provide any information on nearby flow trajectories. Nevertheless, the phase portrait resembles that of a saddle fixed point, with attracting and repelling directions being, respectively, along the x- and y-axes. These axes play the role of the stable and unstable manifolds, respectively, and yet cannot be found by using exponential decay as a criteria. Determining (or even defining) such entities in *unsteady* flows is additionally challenging, but has obvious importance in identifying LCSs in unsteady situations. Note that FTLEs are unlikely to recover such entities, since they do *not* satisfy exponential decay criteria. Explicit *unsteady* examples in both two and three dimensions which possess exactly such nonhyperbolic behaviour could be useful in developing both a theoretical understanding and diagnostic tools for such situations, and

in providing examples to test whether recent tools which do not rely on exponential decay[71–73] can reliably locate such structures.

The idea of seeking invariant manifolds in identifying coherent structures in flows is only several decades old; *vortex structures* have long been investigated as signature coherent entities.[45,76–78] Methods suggested for defining vortices include elliptic versions of the Okubo-Weiss criterion,[79,80] closed or spiralling pathlines,[81] regions of low particle dispersion,[82,83] or stability-based methods.[84,85] It should be noted that topologically elliptic contours of the frozen-time vorticity field do not necessarily correspond to coherent rotational motion in unsteady flows;[85] this highlights the difficulty of imputing coherently rotating Lagrangian motion based on Eulerian properties. If using Lagrangian properties one approach would be to consider the linearised flow around a purported elliptic trajectory, and check for rotational motion around it.[60] This has several difficulties. First, for unsteady flows, the eigenvalues of the frozen-time linearisation do not necessarily correspond to the unsteady motion near the trajectory. Second, even if the flow is steady and thus the eigenvalue criteria may appear legitimate, eigenvalues with zero real part do not necessarily imply pure rotational motion, as is easily verified through the example $\dot{x} = \alpha(x^2 + y^2)x - y$, $\dot{y} = \alpha(x^2 + y^2)y + x$ (this corresponds to $\dot{r} = \alpha r^3, \dot{\theta} = 1$ in polar coordinates). The linearisation around the point $(0, 0)$ has complex conjugate eigenvalues, yet nonlinearities cause nearby behaviour to have potentially different forms: (i) elliptic rotation if $\alpha = 0$, (ii) spiral attraction if $\alpha < 0$, and (iii) spiral repulsion if $\alpha > 0$. To avoid difficulties associated with Eulerian characterisations and degenerate linearisations, this article thinks of an "elliptic trajectory" in the Lagrangian sense as being at the centre of a Lagrangian vortex, carrying along with it adjacent trajectories which are slaved to rotating around it without being attracted or repulsed. This has a pleasing connection to Kolmogorov-Arnold-Moser (KAM) tori in a time-quasiperiodic two-dimensional[86–88] or three-dimensional[89–92] setting, but providing a definition for elliptic trajectories in generically unsteady flows remains elusive. If there were trajectories in an unsteady flow which could be unequivocally identified as being elliptic in the Lagrangian sense, such would offer excellent test examples in the desire to comprehend ellipticity in unsteady flows.[60,81,85,93]

Formulating, improving, and testing diagnostic tools are invaluable in the quest for understanding flow barriers, coherent entities, and fluid transport in real oceanographic, atmospheric, and micro-fluidic flows. In testing such tools, specific examples with explicit flow barriers would be useful, but are not well known because of the theoretical difficulties of determining stable and unstable manifolds, and hyperbolic and elliptic trajectories in unsteady flows. This article offers a class of such unsteady examples, in both two and three dimensions. *Explicit* expressions for the unsteady velocity field, the time-varying elliptic and hyperbolic trajectories, and the stable and unstable manifolds are provided. Even though (by construction) the flow is integrable, the Lagrangian parcel trajectories can be complicated, thereby presenting a nontrivial challenge for diagnostic schemes. It should be emphasised that these examples do *not* possess features such as chaotic mixing or time-dependent transport of fluid between Lagrangian coherent structures which are of paramount interest to understanding fluid motion, but rather provide explicit unsteady solutions (of which there is a paucity) for testing reliability of numerical diagnostics which are being refined for the analysis of precisely such phenomena. The general method for the construction of these examples appears in Sec. II, with two- and three-dimensional examples presented in Secs. III and IV, respectively. The fact that these do indeed satisfy the theoretical requirements for hyperbolicity and stable/unstable manifolds is established in Appendix B. Appendix A provides explanations of the concept of exponential dichotomies, which is key to a theoretical understanding of invariant manifolds in genuinely unsteady systems. While using this theoretical definition in real flows may be impossible, the methods outlined in this article provide insights into its relationship with diagnostic tools. Finally, Secs. V and VI focus on extending these examples in two physically relevant situations: if the hyperbolicity is restricted to finite-time in some way, or if the flow separators are nonhyperbolic.

II. DEFINING UNSTEADY VELOCITY

This section outlines the development of the unsteady velocity field for which the hyperbolic trajectory and its stable and unstable manifolds can be explicitly expressed. Let $\mathbf{x} \in \Omega$, where

Ω is a closed and connected subset of $\mathbb{R}^n$ in which $n = 2$ or 3. This Ω represents the spatial domain available for computational purposes. A *steady* velocity field $\mathbf{u}_0(\mathbf{x})$, which need not be incompressible, is assumed defined in Ω, for which the Lagrangian trajectories are given by

$$\dot{\mathbf{x}} = \mathbf{u}_0(\mathbf{x}). \tag{1}$$

Suppose $\mathbf{m}^*$ is a stagnation point of (1), that is, $\mathbf{u}_0(\mathbf{m}^*) = \mathbf{0}$. Define the Jacobian matrix

$$J = D\mathbf{u}_0\left(\mathbf{m}^*\right), \tag{2}$$

in which the D denotes the spatial derivative. The following *hyperbolicity condition* of the stagnation point $\mathbf{m}^*$ is now assumed:

(2D) If $n = 2$, then J has real eigenvalues λ_s and λ_u such that $\lambda_s < 0 < \lambda_u$.
(3D) If $n = 3$, then the three eigenvalues of J are in one of the following forms:
  (a) they are λ_s^1, λ_s^2, and λ_u, such that $\mathrm{Re}\left(\lambda_s^i\right) < 0$ for $i = 1, 2$, and $\lambda_u > 0$, or
  (b) they are λ_u^1, λ_u^2, and λ_s, such that $\mathrm{Re}\left(\lambda_u^i\right) > 0$ for $i = 1, 2$, and $\lambda_s < 0$.

These conditions guarantee the fact that the stagnation point $\mathbf{m}^*$ possesses both a stable manifold and an unstable manifold. In the three-dimensional case, one of these is two-dimensional and the other is one-dimensional (the theory to be developed also works in 3D if a 2D system satisfying the hyperbolic condition is extended to 3D through the inclusion of $\dot{z} =$ constant; this degenerate situation will not be explicitly discussed). The two-dimensional manifold may be associated with two purely real eigenvalues, or a complex-conjugate pair of eigenvalues which implies rotational behaviour on the manifold. While the eigenvectors of J only define the manifolds locally, the explicit global stable and unstable manifolds of the stagnation point $\mathbf{m}^*$ are assumed known.

Suppose additionally the flow (1) possesses a stagnation point $\mathbf{m}^o$ (i.e., $\mathbf{u}_0(\mathbf{m}^o) = \mathbf{0}$) which has the *ellipticity condition*

(2D) The point $\mathbf{m}^o$ is locally surrounded by a family of periodic orbits of (1).
(3D) There exists a local two-dimensional manifold containing $\mathbf{m}^o$, in which $\mathbf{m}^o$ is surrounded by a family of periodic orbits of (1).

The above definition unambiguously implies rotational motion around $\mathbf{m}^o$ in the *steady* flow (1). A definition based on eigenvalues of $D\mathbf{u}_0(\mathbf{m}^o)$ lying on the imaginary axis is avoided, since this by itself cannot guarantee the desired rotational motion nearby. The definition used here is based on Lagrangian trajectories of (1), sidestepping difficulties associated with Eulerian diagnostics (vorticity, pressure, Okubo-Weiss criterion, rate-of-strain tensor, etc.) since when made unsteady, such definitions require careful consideration (see Sec. 1 in Haller's discussion[85]).

The unsteady flow built from this steady situation involves an arbitrary but invertible *time-dependent* change of coordinates. This will be effected through the family of mappings $\mathbf{Q}_t(\mathbf{x})$ indexed by $t \in \mathbb{R}$, which maps points from Ω to $\mathbb{R}^n$. The following notation will be used for derivatives of $\mathbf{Q}_t(\mathbf{x})$:

$$\dot{\mathbf{Q}}_t(\mathbf{x}) := \frac{\partial \mathbf{Q}_t(\mathbf{x})}{\partial t} \text{ and } D\mathbf{Q}_t(\mathbf{x}) := \frac{\partial \mathbf{Q}_t(x_i)}{\partial x_j} \ (i = 1, \cdots, n; j = 1, \cdots n) \tag{3}$$

in which the latter is the $n \times n$ matrix derivative (Jacobian). Subject to conditions on differentiability and invertibility (which will be satisfied due to the hypothesis to follow), the t-dependent (but spatially independent) matrices $G^{\pm}(t)$ are defined by

$$G^+(t) := D\mathbf{Q}_t\left(\mathbf{m}^*\right) \text{ and } G^-(t) := D\mathbf{Q}_t^{-1}\left(\mathbf{Q}_t\left(\mathbf{m}^*\right)\right), \tag{4}$$

in which $\mathbf{Q}_t^{-1}$ is the mapping inverse to $\mathbf{Q}_t$, which maps points in $\mathbb{R}^n$ from the range of $\mathbf{Q}_t$ to Ω. The following nondegeneracy conditions are imposed on the mappings:

(a) $\mathbf{Q}_t(\mathbf{x})$ has continuous second derivatives in Ω for each $t \in \mathbb{R}$, and continuous first derivatives in t for each $\mathbf{x} \in \Omega$;
(b) $|\det D\mathbf{Q}_t(\mathbf{x})| > 0$ for all $t \in \mathbb{R}$ and $\mathbf{x} \in \Omega$; and

(c) for some constant β satisfying

$$\mathrm{Re}\left(\lambda_s^i\right) < \beta < \mathrm{Re}\left(\lambda_u^i\right) \tag{5}$$

for the eigenvalues of J as described in the hyperbolicity conditions, there exists constants C_1 and C_2 such that the spectral norms (matrix norms) of G^+ and G^- are bounded according to

$$\left\|G^+(t)\right\| \leq C_1 e^{-\beta t} \text{and} \left\|G^-(t)\right\| \leq C_2 e^{\beta t} \tag{6}$$

for all $t \in \mathbb{R}$.

Condition (b) ensures that $\mathbf{Q}_t$ is invertible at each t, and indeed for any $\mathbf{x}$ in the codomain of $\mathbf{Q}_t$,

$$\mathbf{Q}_t\left(\mathbf{Q}_t^{-1}(\mathbf{x})\right) = \mathbf{x}, \tag{7}$$

which upon differentiating with respect to $\mathbf{x}$ and evaluating at $\mathbf{Q}_t(\mathbf{m}^*)$ immediately gives $G^+G^- = \mathbb{I}$ (the identity). The fact that $G^-G^+ = \mathbb{I}$ is similarly obtained by interchanging $\mathbf{Q}_t$ and $\mathbf{Q}_t^{-1}$ in (7), and hence G^+ and G^- are inverses of one another at any $t \in \mathbb{R}$, that is

$$G^-(t) = \left[D\mathbf{Q}_t\left(\mathbf{m}^*\right)\right]^{-1}. \tag{8}$$

Condition (c) requires some explanation. The existence of a β as in (5) is guaranteed, since $\mathrm{Re}\left(\lambda_s^i\right) < 0$ and $\mathrm{Re}\left(\lambda_u^i\right) > 0$ (the superscript i has been included since there may be, say, two eigenvalues with positive real part if $n = 3$; in this case, both these necessarily have the same real value). For example, $\beta = 0$ will always be a legitimate choice, and in this case (6) requires that $G^+(t)$ be chosen such that its, and its inverse's, spectral norms are bounded. However, the less restrictive condition (6), in which one of the norms is permitted to grow exponentially (but with exponential rate controlled by the eigenvalues of J) in forwards time, turns out to be sufficient. It may be worth recalling that the spectral norm (or the "natural" matrix norm, sometimes indicated by $\|\cdot\|_2$) for $n \times n$ real matrices G can be thought of as[94]

$$\|G\| = \sqrt{\text{largest eigenvalue of } \left(G^T G\right)}, \tag{9}$$

in which the superscript T stands for the matrix transpose. More technical details on this norm are available in Appendix A.

Based on these conditions, an *unsteady* velocity field for which any user-specified time-varying hyperbolic/elliptic trajectory exists will now be constructed. This velocity $\mathbf{u}(\mathbf{x}, t)$ and its associated particle paths are defined by

$$\dot{\mathbf{x}} = \mathbf{u}(\mathbf{x}, t) = \dot{\mathbf{Q}}_t\left(\mathbf{Q}_t^{-1}(\mathbf{x})\right) + D\mathbf{Q}_t\left(\mathbf{Q}_t^{-1}(\mathbf{x})\right)\mathbf{u}_0\left(\mathbf{Q}_t^{-1}(\mathbf{x})\right) \tag{10}$$

for all $(\mathbf{x}, t)$ for which $\mathbf{Q}_t^{-1}(\mathbf{x}) \in \Omega$. It is possible to show that for the particular unsteady velocity as given in (10), the time-varying fluid trajectory defined by

$$\mathbf{x}^*(t) = \mathbf{Q}_t\left(\mathbf{m}^*\right) \tag{11}$$

satisfies hyperbolicity. While filling in the details of such hyperbolicity requires a little work (see Appendix B), the basic reason this works is that if the invertible nonlinear transformation

$$\mathbf{m}(t) = \mathbf{Q}_t^{-1}(\mathbf{x}(t)) \tag{12}$$

is applied to (10), then (1) results. In other words, the flow of (10) is steady in a frame moving according to (12), and therefore all flow structures of (1) can be mapped to those in (10) via mapping using (12) and its inverse

$$\mathbf{x}(t) = \mathbf{Q}_t(\mathbf{m}(t)). \tag{13}$$

It is easy to verify that this transformation leads to (10) by taking the t-derivative of (13), by utilising $\dot{\mathbf{m}} = \mathbf{u}_0(\mathbf{m})$ since the $\mathbf{m}$-coordinate satisfies the steady flow (1), and then by substituting for $\mathbf{m}$ in terms of $\mathbf{x}$ from (12). Verification of the fact that (11) is a hyperbolic trajectory in the sense of exponential dichotomies requires more work, and it is here that (6) becomes necessary (details are relegated to Appendix B). Thus, the stable and unstable manifolds of the hyperbolic trajectory

(11) of (10) can be explicitly obtained by applying the inverse transformation (13) to the known manifolds in the **m**-frame.

Now, the elliptic point $\mathbf{m}^o$ under this transformation goes to the trajectory

$$\mathbf{x}^o(t) = \mathbf{Q}_t\left(\mathbf{m}^o\right). \tag{14}$$

Defining ellipticity for trajectories of unsteady flows is contentious (see the discussion by Haller[85]), but (14) corresponds to an elliptic trajectory of (10) in the following sense. The periodic trajectories surrounding the stagnation point $\mathbf{m}^o$ of (1) are mapped by the inverse transformation (13) to a collection of trajectories which circle around $\mathbf{x}^o(t)$. Due to unsteadiness, these do not necessarily form periodic orbits of (10), but still remain slaved to $\mathbf{x}^o(t)$ by the smoothness of the transformation (13). Therefore, in the sense of possessing an open two-dimensional manifold of points surrounding $\mathbf{x}^o(t)$ at each time t which, as time evolves, continues to rotate about $\mathbf{x}^o(t)$, the trajectory $\mathbf{x}^o(t)$ can be thought of as elliptic. Indeed, the transformation (13) includes affine transformations of the form $A(t)\mathbf{x} + \mathbf{b}(t)$ that are used in continuum mechanics to define *objectivity*: a quantity invariant under such a transformation is defined to be objective.[95,96] If a definition for ellipticity is objective, then when $\mathbf{m}^o$ transforms to $\mathbf{x}^o(t)$ under such a transformation, $\mathbf{x}^o(t)$ must also remain elliptic.

A particularly simple sub-case is if $\mathbf{Q}_t(\mathbf{x}) = \mathbf{x} + \mathbf{c}t$; this relates to a moving frame travelling at a constant velocity $\mathbf{c}$. It is worth noting that in this instance the flow (10) is

$$\dot{\mathbf{x}} = \mathbf{u}_0\left(\mathbf{x} - \mathbf{c}t\right) + \mathbf{c}, \tag{15}$$

whose instantaneous stagnation points have nothing to do with the true hyperbolic entity of interest, which is $\mathbf{x}^*(t) = \mathbf{m}^* + \mathbf{c}t$ from (11). This highlights the futility of investigating potential flow regulators in unsteady flows by examining the behaviour of instantaneous stagnation points, which fails even in the simplest situation of a steadily translating frame.

In the full situation for general $\mathbf{Q}_t(\mathbf{x})$, seemingly unruly Lagrangian motion for fluid structures (fluid parcels, hyperbolic/elliptic trajectories, stable/unstable manifolds) can be created, in which the motion of these structures is nevertheless known *exactly*. Such models will form useful testbeds for numerical methods for tracking important flow structures which move unsteadily with time. It should however be noted that arbitrarily complicated transport and mixing is *not* achievable in (10), since the trajectories collectively remain topologically consistent with those of the steady flow (1).

III. 2D EXAMPLES

The Duffing equation is a standard example in nonlinear oscillator theory,[97] but also has been used in fluid mechanics as a testbed for double-gyres[59,63,98–101] and capillary liquid oscillations.[102,103] At its simplest, the steady Duffing flow is given by the steady streamfunction $\psi(x, y) = -\frac{x^2}{2} + \frac{x^4}{4} + \frac{y^2}{2}$ with the associated flow trajectories obeying

$$\left.\begin{aligned} \dot{x} &= \frac{\partial \psi}{\partial y} = y \\ \dot{y} &= -\frac{\partial \psi}{\partial x} = x - x^3 \end{aligned}\right\}. \tag{16}$$

This has a saddle stagnation point at the origin associated with two homoclinic trajectories forming a "bow-tie" manifold structure enclosing two gyres. See Figure 1 for a picture of the streamlines; the flow along all the closed streamlines is in a clockwise sense, and the manifolds are shown by the thick curve. These manifolds are collectively defined by $\psi(x, y) = 0$, that is, by the curve

$$y^2 = x^2\left(1 - \frac{x^2}{2}\right). \tag{17}$$

The Duffing flow (16) also possesses two elliptic points, $\mathbf{m}_1^o \equiv (1, 0)$ and $\mathbf{m}_2^o(-1, 0)$, around which nearby trajectories rotate. Equations (16) and (17) represent the flow in the **m**-frame, with $\mathbf{u}_0$ as given in (16).

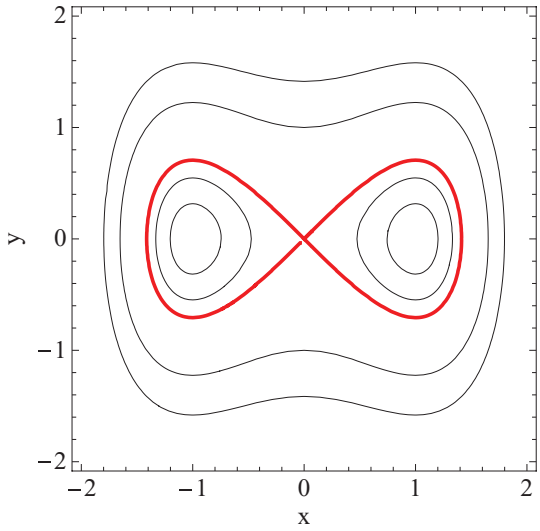

FIG. 1. The flow of the steady version of Duffing's equation (16), with the "bow-tie" manifold structure shown as the thick curve.

As a first example of an unsteady flow derived from this, consider the class of transformations

$$\mathbf{Q}_t(\mathbf{x}) = A(t)\,\mathbf{x} + \mathbf{b}(t) \tag{18}$$

for $n \times n$ matrices A and $n \times 1$ vectors $\mathbf{b}$, both of which are smooth in t. Considering such affine transformations is motivated by the "objectivity criteria" from continuum mechanics; conditions which are invariant under transformations of the form (18) are defined to be "objective," and hence of intrinsic importance.[95,96] It is easy to see that for affine transformations (18), the nondegeneracy conditions are associated with $\det A(t) \neq 0$, and that $G^+(t) = \|A(t)\|$ and $G^-(t) = \|A^{-1}(t)\|$. As a particular example of transformations of the form (18), consider

$$\mathbf{Q}_t(x, y) = (\sin 7t + 2)\begin{pmatrix} \cos \pi t & -\sin \pi t \\ \sin \pi t & \cos \pi t \end{pmatrix}\begin{pmatrix} x \\ y \end{pmatrix} + \begin{pmatrix} t \\ t - \frac{t^2}{3} \end{pmatrix}. \tag{19}$$

In this case, $\det A(t) = (\sin 7t + 2)^2$, $\|A(t)\| = |\sin 7t + 2|$ and $\|A^{-1}(t)\| = |\sin 7t + 2|^{-1}$. The matrix norms are both bounded, and hence satisfy the condition (6) with $\beta = 0$. This form of $A(t)$ achieves rotation with frequency π coupled with pulsation with frequency 7. Using (10), the associated flow is

$$\left.\begin{aligned}
\dot{x} &= \frac{\cos \pi t\left[\left(t^2 - 3t + 3y\right)\cos \pi t + 3\,(t - x)\sin \pi t\right]}{3} - \frac{\pi}{3}\left(t^2 - 3t + 3y\right) - \frac{7\,(t - x)\cos 7t}{\sin 7t + 2} + 1 \\
&\quad - \frac{\sin \pi t\left[\left(3\,(t-x)\cos \pi t - \left(t^2-3t+3y\right)\sin \pi t\right)^3 + 9\left(t^2-3t+3y\right)(\sin 7t+2)^2 \sin \pi t - 27\,(t-x)(\sin 7t+2)^2 \cos \pi t\right]}{27\,(\sin 7t + 2)^2} \\
\dot{y} &= \frac{\sin \pi t\left[\left(t^2 - 3t + 3y\right)\cos \pi t + 3\,(t - x)\sin \pi t\right]}{3} + \pi\,(x - t) - \frac{2t}{3} + \frac{7\left(t^2 - 3t + 3y\right)\cos 7t}{3\,(\sin 7t + 2)} + 1 \\
&\quad + \frac{\cos \pi t\left[\left(3\,(t-x)\cos \pi t - \left(t^2-3t+3y\right)\sin \pi t\right)^3 + 9\left(t^2-3t+3y\right)(\sin 7t+2)^2 \sin \pi t - 27\,(t-x)(\sin 7t+2)^2 \cos \pi t\right]}{27\,(\sin 7t + 2)^2}
\end{aligned}\right\}. \tag{20}$$

The evolution of the elliptic trajectories of (20), from (14), is given by

$$\mathbf{x}^o_{1,2}(t) = \begin{pmatrix} \pm(\sin 7t + 2)\cos \pi t + t \\ \pm(\sin 7t + 2)\sin \pi t + t - \frac{t^2}{3} \end{pmatrix} \tag{21}$$

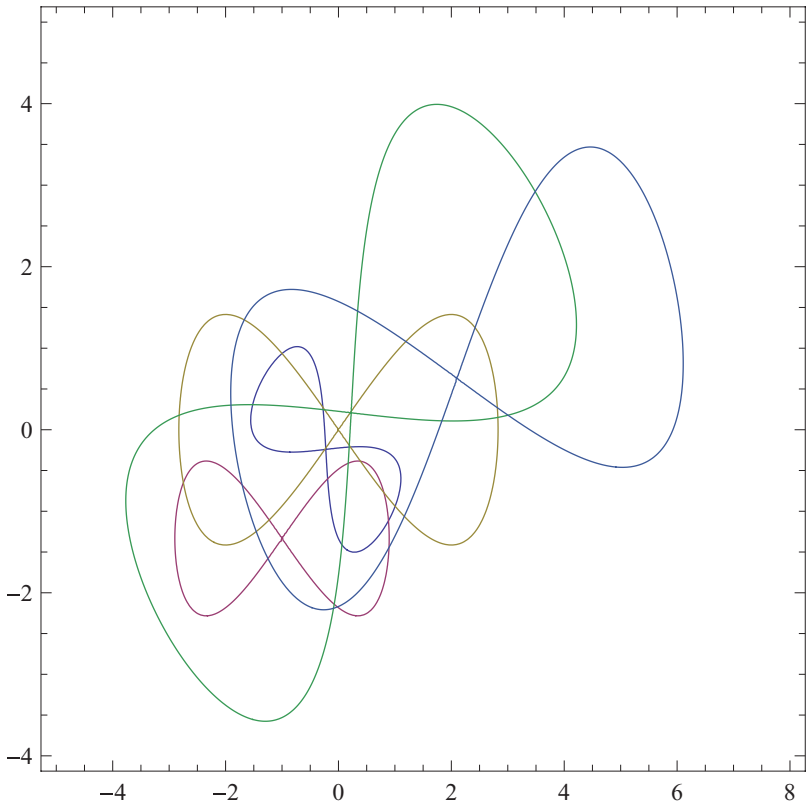

FIG. 2. Five snapshots in time of the manifolds associated with (20) the Duffing equation with transformation (19).

with the plus and minus signs being associated with the elliptic trajectories "1" and "2" respectively. From (11), the hyperbolic trajectory of (20) moves according to

$$\mathbf{x}^*(t) = \begin{pmatrix} t \\ t - \frac{t^2}{3} \end{pmatrix}, \tag{22}$$

and the bow-tie invariant manifolds structure associated with it evolves according to

$$\left[\frac{3(t-x)\sin\pi t + \left(t^2 - 3t + 3y\right)\cos\pi t}{3(x-t)\cos\pi t + \left(t^2 - 3t + 3y\right)\sin\pi t}\right]^2 = 1 - \frac{\left[3(x-t)\cos\pi t + \left(t^2 - 3t + 3y\right)\sin\pi t\right]^2}{18(\sin 7t + 2)^2}. \tag{23}$$

Some time slices of the manifolds as given in (23) are shown in Figure 2 to illustrate these features.

As a second and more general illustration of an unsteady flow, set

$$\mathbf{Q}_t(x, y) = \begin{pmatrix} \tanh(x + e^y \sin t) \\ x - t^2 - 3e^y \end{pmatrix}, \tag{24}$$

a fully nonlinear transformation. This satisfies the nondegeneracy requirements: $\det D\mathbf{Q}_t = -e^y \operatorname{sech}^2(x + e^y \sin t)(3 + \sin t)$ is never zero, and moreover

$$G^+(t) = \begin{pmatrix} \operatorname{sech}^2(\sin t) & \sin t \operatorname{sech}^2(\sin t) \\ 1 & -3 \end{pmatrix} \text{ and } G^-(t) = \frac{1}{3 + \sin t}\begin{pmatrix} 3\cosh^2(\sin t) & \sin t \\ \cosh^2(\sin t) & 1 \end{pmatrix}$$

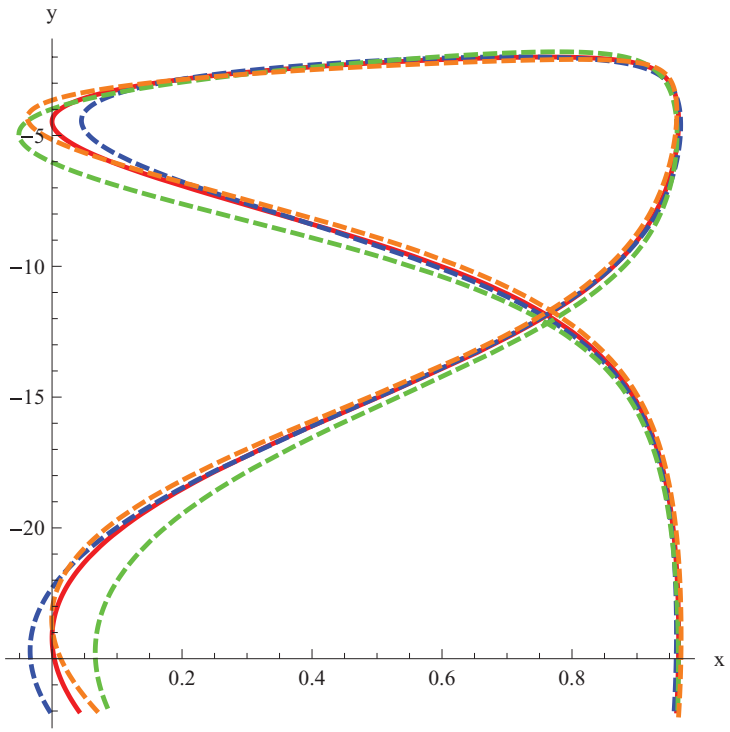

FIG. 3. Evolution of the first elliptic trajectory (solid curve) associated with the transformation (24), and several nearby trajectories (dashed curves).

have bounded entries for all t. The corresponding velocity field associated with this transformation is given by

$$\left.\begin{aligned}
\dot{x} &= \left(1-x^2\right)\left[\ln\frac{\tanh^{-1}x-y-t^2}{3+\sin t}+\frac{\tanh^{-1}x-y-t^2}{3+\sin t}\cos t\right]\\
&\quad+\frac{\left(1-x^2\right)\left(\tanh^{-1}x-y-t^2\right)\left(3\tanh^{-1}x+\left[t^2+y\right]\sin t\right)\left(\left[3+\sin t\right]^2-\left[3\tanh^{-1}x+\left(t^2+y\right)\sin t\right]^2\right)}{(3+\sin t)^4}\\
\dot{y} &= -2t+\ln\frac{\tanh^{-1}x-y-t^2}{3+\sin t}\\
&\quad-\frac{3\left(\tanh^{-1}x-y-t^2\right)\left(3\tanh^{-1}x+\left[t^2+y\right]\sin t\right)\left(\left[3+\sin t\right]^2-\left[3\tanh^{-1}x+\left(t^2+y\right)\sin t\right]^2\right)}{(3+\sin t)^4}
\end{aligned}\right\}. \tag{25}$$

Using (14), it can be shown that the unsteady elliptic trajectories follow the paths

$$\mathbf{x}_1^o(t)=\begin{pmatrix}\tanh\left(1+\sin t\right)\\ -2-t^2\end{pmatrix}\quad\text{and}\quad\mathbf{x}_2^o(t)=\begin{pmatrix}-\tanh\left(1-\sin t\right)\\ -4-t^2\end{pmatrix}. \tag{26}$$

In Figure 3, the evolution of $\mathbf{x}_1^o$ (solid curve) and of several nearby trajectories (dashed curves) are shown. The nearby trajectories remain close for all time, and appear to be "crossing" the elliptic trajectory. Indeed, by construction, all nearby trajectories will revolve around the elliptic trajectory. On the other hand, if only observing the time-evolution of these trajectories, it is difficult to distinguish the elliptic trajectory—hence the difficulty in defining elliptic trajectories for such unsteady situations. The explicit expressions (26) however are exact elliptic trajectories for (25), and can be used for testing assorted numerical diagnostics.

The hyperbolic trajectory associated with the transformation (24) follows

$$\mathbf{x}^*(t)=\begin{pmatrix}\tanh\left(\sin t\right)\\ -3-t^2\end{pmatrix}, \tag{27}$$

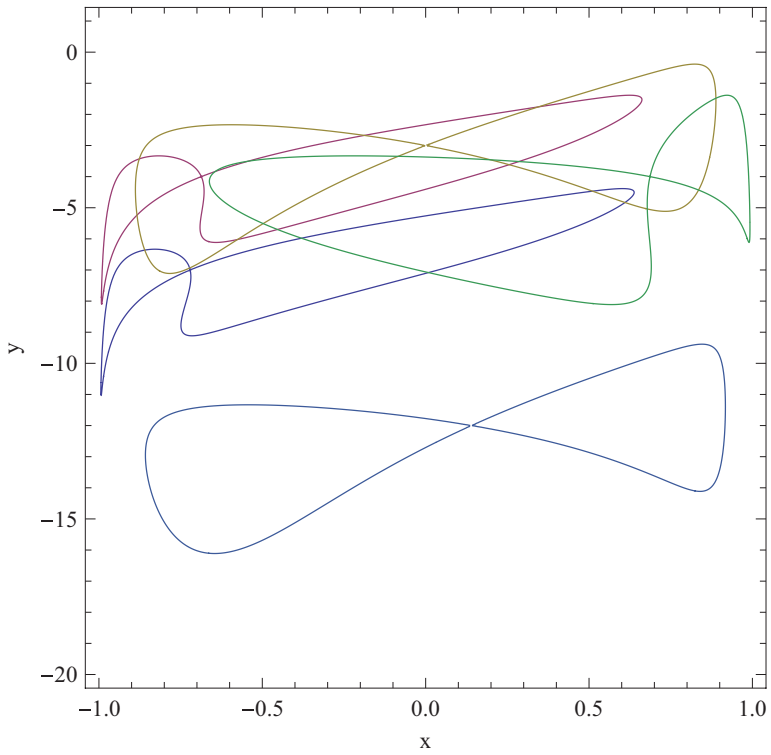

FIG. 4. Several time slices of the heteroclinic manifold structure of the Duffing equation subject to the transformation (24).

and its heteroclinic manifold structure evolves with time explicitly according to

$$(3+\sin t)^2\left(\ln\frac{\tanh^{-1}x-y-t^2}{3+\sin t}\right)^2 = \left(3\tanh^{-1}x+\left[t^2+y\right]\sin t\right)^2\left(1-\frac{\left(3\tanh^{-1}x+\left[t^2+y\right]\sin t\right)^2}{2\,(3+\sin t)^2}\right). \tag{28}$$

Several time slices of these manifolds are shown in Figure 4. A good diagnostic method should be able to recover these explicitly known manifolds, hyperbolic trajectories and elliptic trajectories from the velocity field (25).

IV. 3D EXAMPLES

Hill's spherical vortex[104] is a classical steady three-dimensional entity, and a prototypical example which illustrates the generic integrability[105] of three-dimensional steady Euler flows. While well understood in its simplest form, it continues to be a useful testbed for three-dimensional flows modelling spherical vortices and bubbles,[106–109] their stability,[110–112] transport mechanisms,[22,74,113–115] and visualisation.[116] Most conveniently expressed in terms of a Stokes streamfunction in spherical polar coordinates,[104] the flow of the no-swirl Hill's spherical vortex is expressed in Cartesian coordinates in (C1)+(C2). It has positive parameters c and U with length and velocity dimensions, respectively. The main flow structure of the flow in (C1)+(C2) is illustrated in Figure 5. The flow has two hyperbolic stagnation points, corresponding to the north and the south pole of the sphere $\mathcal{S}$ defined by $x^2+y^2+z^2=c^2$. The north pole has a one-dimensional stable manifold with two branches: $\{(x,y,z)\colon x=y=0 \text{ and } z>c\}$ and $\{(x,y,z)\colon x=y=0 \text{ and } -c<z<c\}$. The first of these is a straight line going to $+\infty$ along the z-axis, while the second lies along the interior axis of $\mathcal{S}$ and approaches the south pole. The north pole also has a two-dimensional unstable manifold

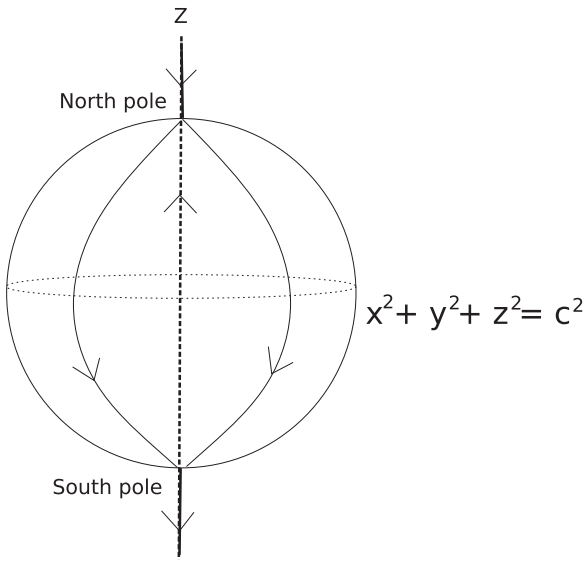

FIG. 5. A schematic of the stagnation points and their invariant manifolds in the steady Hill's spherical vortex.

which is the sphere $\mathcal{S}$ punctured at the poles. The eigenvalue associated with its one-dimensional stable manifold can be easily computed to be $\lambda_s = -3U/c$, and the (repeated) eigenvalue associated with its two-dimensional unstable manifold is $\lambda_u = 3U/(2c)$. Trajectories on this sphere are southwards along the longitudes. The south pole is analogous but with the stability interchanged, with its two-dimensional stable manifold being exactly the unstable manifold of the north pole, and it is a one-dimensional unstable manifold consisting of the branches $\{(x, y, z)\colon x = y = 0 \text{ and } z < -c\}$ and $\{(x, y, z)\colon x = y = 0 \text{ and } -c < z < c\}$, the latter of which coincides with a branch of the stable manifold of the north pole. Thus, the hyperbolic trajectories of the steady flow (C1)+(C2) are the north and south poles, given by

$$\mathbf{x}_n^* = (0, 0, c)^T \text{ and } \mathbf{x}_s^* = (0, 0, -c)^T, \tag{29}$$

in which the subscripts represent the *n*orth and *s*outh hyperbolic trajectories. The associated two-dimensional manifold structure is a heteroclinic manifold connecting the two hyperbolic points in (29), and given by

$$x^2 + y^2 + z^2 = c^2, \tag{30}$$

in which the points associated with (29) need to be excluded. The one-dimensional manifold is the z-axis, once again excluding the hyperbolic points.

Hill's spherical vortex also possesses a ring of stagnation points given by the curve

$$\mathcal{E} = \left\{(x, y, z) : z = 0 \text{ and } x^2 + y^2 = \frac{c^2}{2}\right\}. \tag{31}$$

The axisymmetry of Hill's spherical vortex ensures that the trajectories in each azimuthal plane are identical, and since $\mathcal{E}$ intersects such a plane at exactly one point around which there is a one-parameter family of periodic trajectories, each point of $\mathcal{E}$ may be considered elliptic. For a chosen transformation leading to an unsteady flow (10), it is now easy to determine the hyperbolic, elliptic, and invariant manifold structures.

As a first example, suppose

$$\mathbf{Q}_t(x, y, z) = \begin{pmatrix} -2 & 7 - 5\cos\frac{Ut}{c} & 0 \\ 1 & 4 & 0 \\ 0 & 0 & -3 \end{pmatrix} \begin{pmatrix} 2 + \sin\frac{Ut}{c} & 0 & 0 \\ 0 & 3 - \cos\frac{4Ut}{c} & 0 \\ 0 & 0 & 7 \end{pmatrix} \begin{pmatrix} x \\ y \\ z \end{pmatrix} + \begin{pmatrix} c\cos\frac{Ut}{c} \\ 3c\sin\frac{Ut}{c\sqrt{2}} \\ \frac{2c^2}{\sqrt{c^2+U^2t^2}} \end{pmatrix}, \tag{32}$$

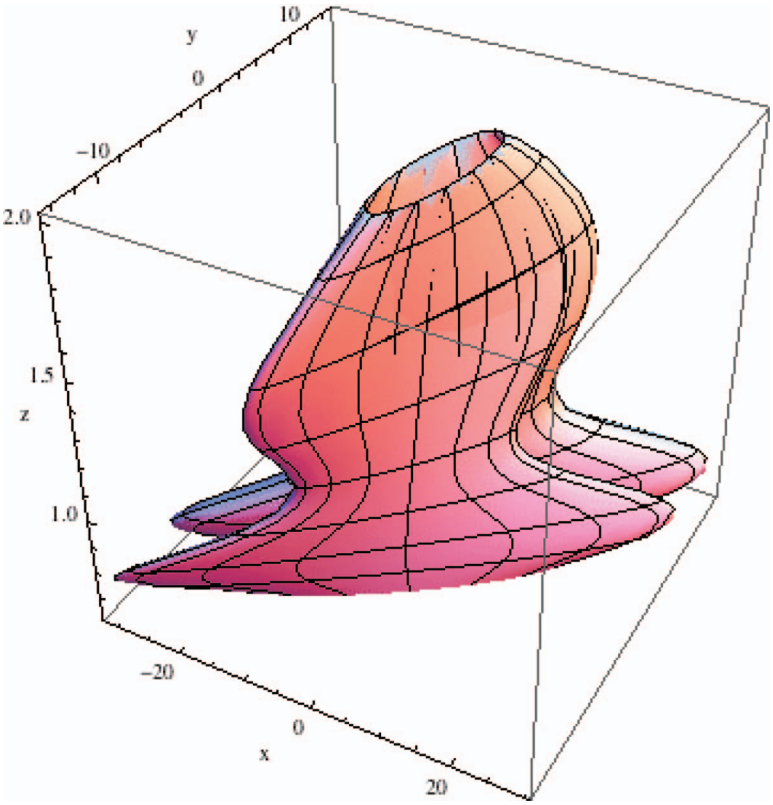

FIG. 6. The evolution of the ring of elliptic points in Hill's spherical vortex transformed using (32), that is, for the flow given by (C3)+(C4), for the parameter choice $U = 1$, $c = 1$, $\mu = -1/2$, and $\omega = 2\pi$.

which is in the form of transformation (18) related to objectivity. Now

$$\det D\mathbf{Q}_t = 105\left(3 - \cos\frac{Ut}{c}\right)\left(2 + \sin\frac{Ut}{c}\right)\left(3 - \cos\frac{4Ut}{c}\right)$$

is never zero, and moreover $\|G^{\pm}(t)\|$ is bounded for all t since each matrix consists of bounded elements. This is hence a legitimate transformation to use, and its associated unsteady velocity field is given in (C3)+(C4). Important features of this unsteady flow can now be expressed explicitly by applying the transformation $\mathbf{Q}_t$ to the corresponding known entities of the steady flow (C1)+(C2). For example, the family of elliptic points, parametrised by $\theta \in [0, 2\pi)$, follows the trajectories

$$\mathbf{x}_\theta^o(t) = \begin{pmatrix} \sqrt{2}c\cos\theta\left(\sin\left(\frac{tU}{c}\right) + 2\right) + \frac{c\sin\theta\left(5\cos\left(\frac{tU}{c}\right) - 7\right)\left(\cos\left(\frac{4tU}{c}\right) - 3\right)}{\sqrt{2}} + c\cos\left(\frac{tU}{c}\right) \\ \frac{c\cos\theta\left(\sin\left(\frac{tU}{c}\right) + 2\right)}{\sqrt{2}} - 2\sqrt{2}c\sin\theta\left(\cos\left(\frac{4tU}{c}\right) - 3\right) + 3c\sin\left(\frac{tU}{\sqrt{2}c}\right) \\ \frac{2c}{\sqrt{\frac{t^2U^2}{c^2} + 1}} \end{pmatrix}. \tag{33}$$

The surface traced out by evolving these elliptic points in time is shown in Figure 6. The two hyperbolic trajectories are

$$\mathbf{x}_n^*(t) = \begin{pmatrix} c\cos\frac{Ut}{c} \\ 3c\sin\frac{Ut}{c\sqrt{2}} \\ -21c + \frac{2c^2}{\sqrt{c^2 + U^2t^2}} \end{pmatrix} \text{ and } \mathbf{x}_s^*(t) = \begin{pmatrix} c\cos\frac{Ut}{c} \\ 3c\sin\frac{Ut}{c\sqrt{2}} \\ 21c + \frac{2c^2}{\sqrt{c^2 + U^2t^2}} \end{pmatrix}, \tag{34}$$

and the two-dimensional heteroclinic manifold structure evolves according to

$$\left(\frac{z-\frac{2c^2}{\sqrt{c^2+U^2t^2}}}{21}\right)^2+\left(\frac{x+2y-c\cos\frac{Ut}{c}-6c\sin\frac{Ut}{c\sqrt{2}}}{5\left(\cos\frac{Ut}{c}-3\right)\left(\cos\frac{4Ut}{c}-3\right)}\right)^2$$
$$+\left(\frac{4x-7y+21c\sin\frac{Ut}{c\sqrt{2}}+\cos\frac{Ut}{c}\left[5y-4c-15c\sin\frac{Ut}{c\sqrt{2}}\right]}{5\left(\cos\frac{Ut}{c}-3\right)\left(2+\sin\frac{Ut}{c}\right)}\right)^2=c^2. \tag{35}$$

While this is an ellipsoid at each instance in time, its axis lengths and orientations are changing with respect to time. This was accomplished by using a product of two matrices in the transformation (32): the second (diagonal) matrix causes the axis lengths to pulsate, while the first matrix provides a mechanism for the relative orientation between the axes to change quasi-periodically. Meanwhile, the one-dimensional part of the manifold structure continues to be the straight line connecting the two hyperbolic trajectories, and can be represented parametrically by

$$\mathbf{r}(s,t)=\begin{pmatrix} c\cos\frac{Ut}{c} \\ 3c\sin\frac{Ut}{c\sqrt{2}} \\ \frac{2c^2}{\sqrt{c^2+U^2t^2}}-21s \end{pmatrix} \tag{36}$$

at each instance in time t, in which $s\in\mathbb{R}$ is the parametric coordinate.

As a second example which corresponds to a genuinely nonlinear transformation, consider

$$\mathbf{Q}_t(x,y,z)=\begin{pmatrix} \frac{e^{\mu t}}{c^4}(z-3c)(x+3c)^3 \\ e^{\mu t}(2+\cos(\omega t))\tan^{-1}\frac{y}{4c} \\ e^{\mu t}e^{z/c} \end{pmatrix}, \tag{37}$$

in which μ and ω are two parameters. It can be shown that invertibility is satisfied within the time-varying domain

$$\left[\left(\frac{xe^{-\mu t}}{\log z-3-t\mu}\right)^{1/3}-3\right]^2+\left[\ln\left(ze^{-\mu t}\right)\right]^2+16\tan^2\frac{ye^{-\mu t}}{2+\cos\omega t}<4, \tag{38}$$

which is a subset of $z>0$; see Appendix C. For the two hyperbolic trajectories, one can calculate that

$$\left\|G^+_{n,s}(t)\right\|=K^+_{n,s}\frac{1}{c^2}e^{2\mu t}\quad\text{and}\quad\left\|G^-_{n,s}(t)\right\|\le K^-_{n,s}c^2e^{-2\mu t} \tag{39}$$

for explicit constants $K^\pm_{n,s}$ as shown in Appendix C. Thus, the nondegeneracy condition (6) is achievable if μ is chosen to satisfy

$$-\frac{3U}{4c}<\mu<\frac{3U}{4c}. \tag{40}$$

The velocity field corresponding to this transformation is given in equations (C8)+(C9), and the following discussion on flow structures is in relation to this unsteady flow. The evolution of the family of elliptic trajectories can be given explicitly by

$$\mathbf{x}^o_\theta(t)=\begin{pmatrix} -\frac{3}{8}e^{\mu t}\left(6+\sqrt{2}\cos\theta\right)^3 \\ e^{\mu t}(2+\cos\omega t)\tan^{-1}\left(\frac{\sin\theta}{4\sqrt{2}}\right) \\ e^{\mu t} \end{pmatrix}. \tag{41}$$

The relevant hyperbolic trajectories are

$$\mathbf{x}^*_n(t)=\begin{pmatrix} -54\,e^{\mu t} \\ 0 \\ e^{\mu t+1} \end{pmatrix}\quad\text{and}\quad\mathbf{x}^*_s(t)=\begin{pmatrix} -108\,e^{\mu t} \\ 0 \\ e^{\mu t-1} \end{pmatrix}, \tag{42}$$

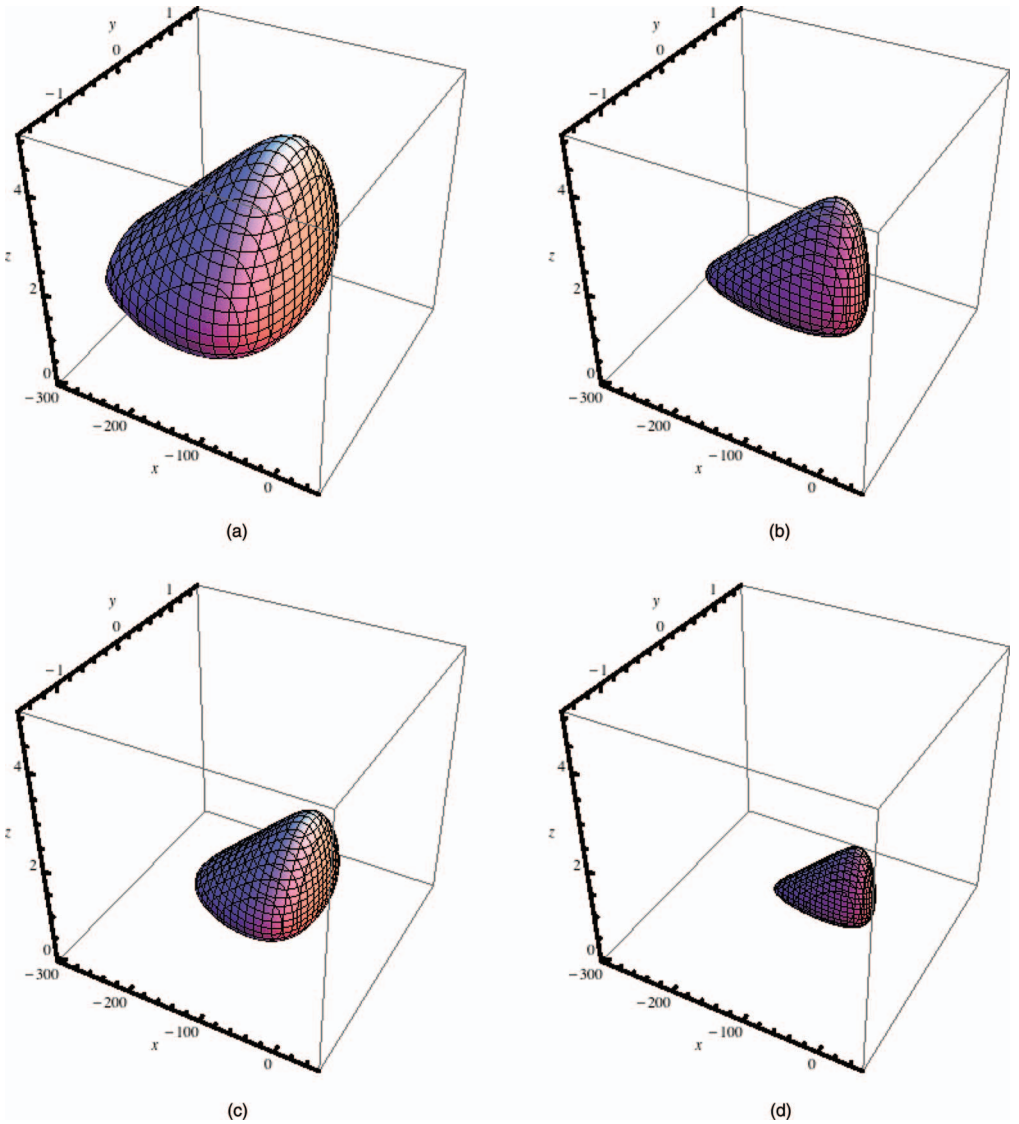

FIG. 7. The heteroclinic manifold for Hill's spherical vortex transformed using (32), that is, for the flow given by (C3)+(C4), for the parameter choice $U = 1$, $c = 1$, $\mu = -1/2$, and $\omega = 2\pi$. The four panels show (a) $t = -1$, (b) $t = -0.5$, (c) $t = 0$, and (d) $t = 0.5$.

and the two-dimensional heteroclinic manifold structure evolves according to

$$\left[\left(\frac{xe^{-\mu t}}{\log z - 3 - t\mu}\right)^{1/3} - 3\right]^2 + \left[\ln\left(ze^{-\mu t}\right)\right]^2 + 16\tan^2\frac{ye^{-\mu t}}{2+\cos\omega t} = 1. \tag{43}$$

This is now not a standard ellipsoid at each time instance, but a more general closed surface. Illustrations of the heteroclinic structure is presented in Figure 7 at various instances in time. The one-dimensional manifold structure (the z-axis in the steady Hill's flow) for the unsteady flow (C8)+(C9) is the curve given parametrically by

$$\mathbf{r}(s,t) = \begin{pmatrix} \frac{27(s-3c)e^{\mu t}}{c} \\ 0 \\ e^{s/c}e^{\mu t} \end{pmatrix}, \tag{44}$$

where $s \in \mathbb{R}$ is the parameter. This is now a curved entity at each time t.

V. FINITE-TIME CONSTRUCTIONS

As well understood, real flows (observational data, or experimentally or numerically generated velocity fields) are by their very nature not infinite-time objects. However, for a theoretical definition of hyperbolic trajectories, exponential decay estimates as time progresses to infinity are needed (see Appendix A). Obtaining *finite-time* versions of these definitions, applicable for example in real flows in which flow barriers appear to exist on the meso-scale, continues to be an intense area of study.[5,22,55,57,64] Asserting that the exponential dichotomy estimates in (A4) occur only on finite times[5,22] is equivalent to the statement that the relevant quantities are bounded by choosing the prefactors in (A4) to be sufficiently large, which then fails to pick up on decay rates. One approach is to define Lagrangian coherent structures[42,55,57] (which are proxies for manifolds), typically defined as entities associated with maximum decay rates over a specified time. Many other diagnostic techniques for identifying flow barriers have their own versions designed for different types of finite time limitations.[20,37,60,63,70,74] Several theoretical methods also venture into the finite-time realm, but differ in their interpretation of what finite-time means. Some deal with flow maps over a finite duration,[55,70,117] others examine flows which diverge from an infinite-time flow field in some specified time-dependent fashion[23,118] and yet others focus on issues of defining finite-time hyperbolicity.[55,119,120] These offer several ideas on how to extend the infinite-time models constructed previously to finite-time situations.

A. Departing forms

Any numerical method is of necessity confined to some finite closed spatial domain, say S. If $\mathbf{Q}_t$ in constructing $\mathbf{u}$ is chosen so that a relevant hyperbolic trajectory *leaves* S at a certain time instance, this can be construed a temporary hyperbolic structure in relation to S. This can be easily realised by choosing an additive term in $\mathbf{Q}_t$ which is unbounded in time, as in the first Duffing example (19) which results in an unbounded hyperbolic trajectory (22). Now if the computational domain were $S = [-10, 10] \times [-10, 10]$, say, the hyperbolic trajectory would exit S by $t = 10$. A strong diagnostic method should be able to capture these structures while they are within the computational domain. This scenario can be complicated by choosing an additive term such that the hyperbolic trajectory departs from S and then returns, possibly repeating this process several times.

B. Transitory forms

Here, one takes any of the models built previously, with velocity field $\mathbf{u}(\mathbf{x}, t)$, and adds it to a known steady flow $\mathbf{U}(\mathbf{x})$ in a transitory way. This is achieved by setting $\mathbf{u}$ to zero outside a finite interval $[T_1, T_2]$, i.e.,

$$\dot{\mathbf{x}} = \mathbf{U}(\mathbf{x}) + [H(t - T_1) - H(t - T_2)]\,\mathbf{u}(\mathbf{x}, t), \tag{45}$$

in which H is the Heaviside (unit-step) function. This accomplishes the appearance of the relevant hyperbolic structure within the time $[T_1, T_2]$, on top of any such structures that exist for all time corresponding to $\mathbf{U}$. While the transitory structures do not obey exponential dichotomy conditions, models of the form (45) form a nice paradigm for transitory hyperbolic structures in 2D or 3D flows. One could, of course, add arbitrarily many such transitory elements to (45), operating over different time intervals at different locations. Such "transitorily hyperbolic" trajectories will satisfy finite-time diagnostics such as mesohyperbolicity,[60] which attempts to identify trajectories which are hyperbolic on average over a given time interval. Smoother transitory structures are obtainable by replacing the box function $H(t - T_1) - H(t - T_2)$ in (45) by a smoothened version, which either decays only at infinity (e.g., a Gaussian), or which smoothly approaches zero at finite endpoints. An interesting scenario emerges if this function were replaced by $\sin \omega t$; within each sign definite time-interval associated with this, there would be transitorily hyperbolic decay, which then reverses direction in the next time interval.

Such examples are suggestive testbeds for practitioners seeking explicit examples for testing diagnostic methods for locating finite-time manifolds. Whatever their definition happens to be, these

do act as temporary flow barriers or regulators, and the methods of this article apparently offer a method for developing explicit examples which mimic this behaviour in a certain way.

VI. NONHYPERBOLIC CONSTRUCTIONS

As discussed in the Introduction, there is another class of important flow separators which has relevance in flows: those which are *nonhyperbolic*. To the author's knowledge, there is as yet no accepted definition for these entities in unsteady flows. Since many diagnostic methods (in particular, finite-time Lyapunov exponents) use exponential decay as an essential part of their algorithm, these too are unlikely to recover these flow barriers. By modifying the examples of this article, it is possible to generate models which by construction have nonhyperbolic time-varying trajectories which have attached to them flow separating invariant manifolds.

A. Nonhyperbolicity in steady flow

For the steady flow $\mathbf{u}_0(\mathbf{x})$, consider the system $\dot{x} = -x^3$, $\dot{y} = y^3$ as discussed in the Introduction; this possesses a saddle-like stagnation point at (0, 0) which is nevertheless not hyperbolic in the sense of the linearisation matrix J. Consider an invertible map $\mathbf{Q}_t(\mathbf{x})$ which does not necessarily satisfy the nondegeneracy condition (6), from which an unsteady flow (10) is generated. For example, either of the maps (19) or (24) could be used for $\mathbf{Q}_t(\mathbf{x})$. Now, flow structures of the steady flow are mapped to those of the unsteady flow, and thus $\mathbf{Q}_t(\mathbf{0})$ is a specialised trajectory of (10) to which is attached important flow separators: $\mathbf{Q}_t(x\text{-axis})$ is the stable manifold and $\mathbf{Q}_t(y\text{-axis})$ the unstable manifold. These are nonhyperbolic in general, and cannot be defined theoretically or identified diagnostically by using exponential decays, but are still flow barriers. A similar construction can be made for a three-dimensional example, by starting with a steady situation with degenerate linearisation and applying a transformation $\mathbf{Q}_t(\mathbf{x})$ to it.

As a specific example of such a construct, consider the following modification of the Duffing flow, which shall be called the nonhyperbolic Duffing flow:

$$\left.\begin{aligned} \dot{x} &= y \\ \dot{y} &= x^3 - x^5 \end{aligned}\right\}. \tag{46}$$

The stagnation point $\mathbf{x}^*$ at the origin is nonhyperbolic, but the nearby behaviour is easily obtained since (46) is associated with a steady streamfunction $\psi(x, y) = -\frac{x^4}{4} + \frac{x^6}{6} + \frac{y^2}{2}$, whose contours are shown in Figure 8. The important separating curve between the interior vortices and the exterior is given by $\psi(x, y) = 0$, and is indicated by the bold red curve which becomes tangential to itself at the origin. This is the "heteroclinic structure" associated with the nonhyperbolic point $\mathbf{x}^* = (0, 0)$, which is nonetheless an important flow trajectory since its accompanying manifolds form an important flow boundary. The elliptic trajectories of (46) are the points $(-1, 0)$ and $(1, 0)$ as before. Now, suppose the transformation (24) were used, leading to the unsteady flow

$$\left.\begin{aligned} \dot{x} &= \frac{(1-x^2)\sin t\left(\tanh^{-1}x - y - t^2\right)\left([3+\sin t]^2 - \left[(t^2+y)\sin t + 3\tanh^{-1}x\right]^2\right)\left([t^2+y]\sin t + 3\tanh^{-1}x\right)^3}{(3+\sin t)^6} \\ &\quad + \left(1-x^2\right)\left[\ln\frac{\tanh^{-1}x - y - t^2}{3+\sin t} + \frac{\cos t\left(\tanh^{-1}x - y - t^2\right)}{3+\sin t}\right] \\ \dot{y} &= -2t + \ln\frac{\tanh^{-1}x - y - t^2}{3+\sin t} \\ &\quad + \frac{3\left(y + t^2 - \tanh^{-1}x\right)\left([3+\sin t]^2 - \left[(t^2+y)\sin t + 3\tanh^{-1}x\right]^2\right)\left([t^2+y]\sin t + 3\tanh^{-1}x\right)^3}{(3+\sin t)^6} \end{aligned}\right\}. \tag{47}$$

Using (14), it can be shown that the unsteady elliptic trajectories of (47) follow the paths

$$\mathbf{x}_1^o(t) = \begin{pmatrix} \tanh(1+\sin t) \\ -2 - t^2 \end{pmatrix} \text{ and } \mathbf{x}_2^o(t) = \begin{pmatrix} -\tanh(1-\sin t) \\ -4 - t^2 \end{pmatrix}. \tag{48}$$

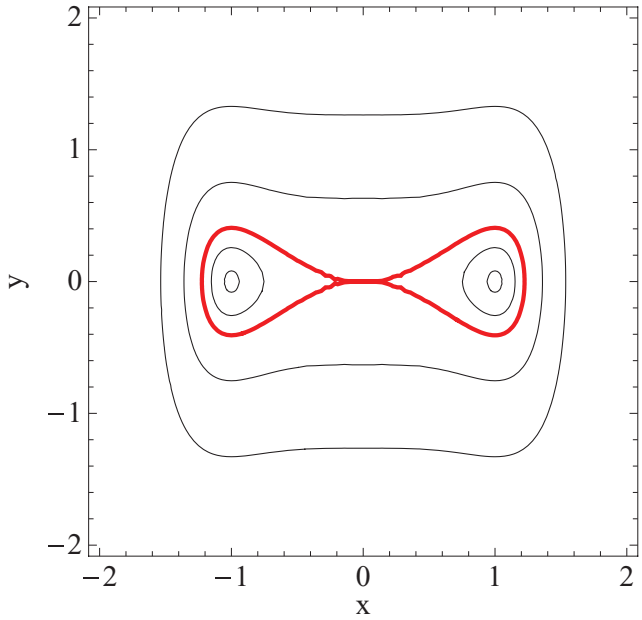

FIG. 8. The flow of the steady version of the nonhyperbolic Duffing equation (46), with deformed bow-tie manifold structure shown as the thick curve.

The specialised trajectory playing the role of the hyperbolic trajectory of (47) follows

$$\mathbf{x}^*(t) = \begin{pmatrix} \tanh(\sin t) \\ -3 - t^2 \end{pmatrix}, \tag{49}$$

and its heteroclinic manifold structure evolves with time explicitly according to

$$\begin{aligned} &(3+\sin t)^4 \left(\ln \frac{\tanh^{-1} x - y - t^2}{3+\sin t} \right)^2 \\ &\quad = \left(3\tanh^{-1} x + \left[t^2 + y\right]\sin t\right)^4 \left(\frac{1}{2} - \frac{\left(3\tanh^{-1} x + \left[t^2+y\right]\sin t\right)^2}{3\,(3+\sin t)^2} \right). \end{aligned} \tag{50}$$

These are important flow structures in the flow (47), demarcating regions of distinct motion and hence identifying LCSs associated with (47). Nevertheless, they *cannot* be recovered using techniques such as FTLEs since exponential decay does not occur; (49) is not hyperbolic in the sense of exponential dichotomies. An interesting question would be whether any diagnostic technique could recover these nonhyperbolic flow separating entities.

B. Nonhyperbolicity in transformation

If the nondegeneracy conditions (5) and (6) were *not* satisfied, the proof of hyperbolicity (as established in Appendix B) would fail. The second map (37) used to adapt Hill's spherical vortex gives an immediate example: if one chooses μ to *not* satisfy (40), then hyperbolicity is not inherited by the transformed northern and southern specialised trajectories. On the other hand, these trajectories continue to be important players in the unsteady flow (C8)+(C9), since they live in the congruence of the important flow separators (43) and (44). Commonly used methods such as finite-time Lyapunov exponents are unlikely to recover these flow structures since they are unrelated to exponential decay. The efficacy of more recently developed methods such as minimum curve length increase,[72] ergodic quotient,[74] finite-time entropy,[73] topological braids,[71] or Perron-Frobenius/Koopman operator methods[61,65–70] on locating nonhyperbolic but significant trajectories can be tested through this example in which μ does not satisfy (40).

The first of these methods is particularly easy to implement to create unsteady nonhyperbolic invariant manifolds, which would form excellent examples for testing diagnostic methods' efficacy in recovering nonhyperbolic flow entities. Recently, developing methods which do not necessarily create their algorithms based on exponential decay rates[71–74] are possible contenders; establishing ability to recover nonhyperbolic Lagrangian coherent structures would enhance their applicability. These classes of models could also be useful in helping *define* such nonhyperbolic flow separators in unsteady flows.

VII. CONCLUDING REMARKS

With a view to providing testbeds for elliptic trajectories, hyperbolic trajectories and their invariant manifolds in genuinely unsteady two- and three-dimensional flows, this article has so far outlined a method for developing an explicit class of such examples in *infinite-time* situations. By following the construction of an unsteady flow as given in (10), it is possible to obtain explicit expressions for the time evolution of these important flow entities. Since the *definition* of a hyperbolic trajectory—the unsteady analogue of a stagnation point—is not obvious in many instances, a careful explanation of such a definition (in terms of exponential dichotomies) has been provided in Appendix A. While this definition is extremely difficult to use in any given flow, it was shown that the specific trajectories generated by the methods of this article were indeed hyperbolic. A variety of examples has been given, which can easily be built upon by following the procedure outlined if more complicated examples are needed. It should be noted that the class of examples in this article is developed specifically from steady flows, and as such does *not* provide examples in which chaotic mixing occurs, even though complicated Lagrangian trajectories can be achieved by choosing complicated maps $\mathbf{Q}_t(\mathbf{x})$ in (10).

The preceding discussion indicates that the models developed here can be extended in several ways with hardly any additional work. First, any known steady flow which has desired flow kinematics can be used for the steady Euler flow $\mathbf{u}_0$, and corresponding unsteady flows generated from (10). Second, the freedom of choosing the maps $\mathbf{Q}_t(\mathbf{x})$ enables one to exemplify a large range of behaviours (such as highly oscillatory hyperbolic trajectories, time scale separations in rotation/translation/axis-reorientation, seemingly erratic flow trajectories, warping of invariant manifolds, etc). Third, the models are easily extended to finite-time and nonhyperbolic situations as discussed in Secs. V and VI, providing explicit knowledge of important flow structures in a more realistic class of problems for which theoretical and diagnostic methods are continuing to be developed. This class of models can therefore be highly useful as more sophisticated diagnostic tools are developed in the quest for understanding flow barriers in complex time-varying two- and three-dimensional flows.

ACKNOWLEDGMENTS

Support from Connecticut College through the R.F. Johnson Fund and the Research Matters initiative are gratefully acknowledged.

APPENDIX A: TECHNICAL DEFINITIONS

1. Hyperbolicity

The idea is to decide whether trajectory $\mathbf{x}^*(t)$ of a general unsteady (non-autonomous) n-dimensional system

$$\dot{\mathbf{x}} = \mathbf{u}(\mathbf{x}, t) \tag{A1}$$

is hyperbolic. To examine "nearby" motion, define a solution to (A1) by $\mathbf{x}(t) = \mathbf{x}^*(t) + \mathbf{y}(t)$, and confine attention to when $\mathbf{y}(t)$ is small (i.e., *linearise around* $\mathbf{x}^*(t)$). Substituting in (A1), utilising Taylor expansions along with the fact that $\mathbf{x}^*(t)$ is also a solution to (A1), and neglecting terms of order $|\mathbf{y}|^2$ leads to the *variational system*

$$\dot{\mathbf{y}} = D\mathbf{u}\left(\mathbf{x}^*(t), t\right)\mathbf{y}. \tag{A2}$$

The matrix derivative $D\mathbf{u}$ above is evaluated along the purported hyperbolic trajectory $\mathbf{x}^*(t)$ and general time t. Now, the definition for a trajectory being hyperbolic is:

- A solution $\mathbf{x}^*(t)$ of (A1) is a *hyperbolic trajectory* of (A1) if its variational system (A2) possesses an *exponential dichotomy*, with projection matrix P being neither the identity nor the zero matrix.

2. Exponential dichotomies

A linear system of the form

$$\dot{\mathbf{y}} = B(t)\,\mathbf{y} \tag{A3}$$

for a time-varying $n \times n$ matrix $B(t)$ is said to possess an *exponential dichotomy*[16,39,40] if there exists an $n \times n$ projection matrix P and positive constants K_1, K_2, α_1, and α_2 such that a $n \times n$ *fundamental matrix solution* $Y(t)$ to (A3) satisfies

$$\left.\begin{aligned} \left\| Y(t) P Y^{-1}(s) \right\| &\leq K_1\, e^{-\alpha_1 (t-s)} \text{ for } t \geq s \text{ and} \\ \left\| Y(t) (\mathbb{I} - P) Y^{-1}(s) \right\| &\leq K_2\, e^{-\alpha_2 (s-t)} \text{ for } s \geq t \end{aligned}\right\}. \tag{A4}$$

3. Fundamental matrix solution

The fundamental matrix solution $Y(t)$ of (A3) is the $n \times n$ matrix solution to

$$\dot{Y} = B(t)\,Y(t),\, Y(s) = Y_s. \tag{A5}$$

The "initial" condition for the matrix is posed at $t = s$, and the matrix initial condition Y_s is assumed to possess linearly independent columns. Since the evolution of each of the linearly independent column vectors of Y_s (which form a basis for $\mathbb{R}^n$) are simultaneously captured in the fundamental matrix solution $Y(t)$ of (A5), *all* solutions to (A3) are captured by $Y(t)$. If $\mathbf{y}(s) = \mathbf{y}_s$ is any $n \times 1$ vector initial condition to (A3), it is easy to verify that the corresponding solution at time t to (A3) can be expressed in terms of the fundamental matrix solution by

$$\mathbf{y}(t) = Y(t)\,Y^{-1}(s)\,\mathbf{y}_s. \tag{A6}$$

4. Matrix norm

The matrix norm used in (A4) is the "2-norm" induced by the standard Euclidean norm on vectors in $\mathbb{R}^n$. For $n \times n$ matrices G, this norm is defined by

$$\|G\| = \sup_{\mathbf{w} \neq \mathbf{0}} \frac{\|G\mathbf{w}\|}{\|\mathbf{w}\|}. \tag{A7}$$

The "sup" indicates the "supremum" over all vectors in $\mathbb{R}^n$, and each of the norms on the right-hand side of (A7), being applied to vectors in $\mathbb{R}^n$, is the standard Euclidean "2-norm" (distance norm) given component-wise by

$$\|\mathbf{w}\| = \sqrt{w_1^2 + w_2^2 + \cdots + w_n^2}. \tag{A8}$$

It turns out[94] that for real matrices, the definition (A7) is equivalent to (9), that is, the square-root of the largest eigenvalue of $G^T G$. (It should be noted that the eigenvalues of $G^T G$ are real and non-negative.)

5. Projections and intuition regarding exponential dichotomies

The $n \times n$ matrix P is a *projection* defined by $P^2 = P$, and is associated with the projection operator to the stable manifold at time s. The constant α_1 is the decay rate associated with the stable

manifold, as can be seen as follows. If $\mathbf{w}$ is an arbitrary $n \times 1$ vector and if $t \geq s$, then

$$\begin{aligned} \left\| Y(t)Y^{-1}(s)Y(s)P\mathbf{w} \right\| &= \|Y(t)P\mathbf{w}\| = \|Y(t)PP\mathbf{w}\| = \left\| Y(t)PY^{-1}(s)Y(s)P\mathbf{w} \right\| \\ &\leq \left\| Y(t)PY^{-1}(s) \right\| \, \|Y(s)P\mathbf{w}\| \\ &\leq K_1 e^{-\alpha_1(t-s)} \, \|Y(s)P\mathbf{w}\| \,, \end{aligned} \tag{A9}$$

where the second and third equalities use the fact that $P^2 = P$ and $Y^{-1}Y = I$, the next inequality utilises the matrix norm as defined in (A7) applied to the matrix $Y(t)PY^{-1}(s)$ and the vector $Y(s)P\mathbf{w}$, and the final inequality the first exponential dichotomy condition (A4). Now, imagine (A3) subject to the initial condition $\mathbf{y}(s) = Y(s)P\mathbf{w}$. Then, using (A6) and (A9) can be written as

$$\|\mathbf{y}(t)\| \leq K_1 e^{-\alpha_1(t-s)} \, \|\mathbf{y}(s)\| \text{ if} t \geq s. \tag{A10}$$

This gives a pleasing intuitive interpretation of the first exponential dichotomy condition in (A4). The solution $\mathbf{y}(t)$ corresponding to an initial condition chosen in the range of P, decays exponentially with t. Thus, in the time slice $t = s$, P projects onto the stable manifold. In the *autonomous* situation (that is, if $B(t)$ in (A3) does not depend on t), the α_1 in (A10) is associated with the stable eigenvalue(s) of B. This is relevant to the original steady flow (1) that forms the backbone for the unsteady flows constructed in this article, since the linearisation of (1) about the stagnation point $\mathbf{m}^*$ is

$$\dot{\mathbf{y}} = J\,\mathbf{y}, \tag{A11}$$

which is in the form of (A3) with $B(t) = J$. Here, (A10) can be interpreted with $\alpha_1 = -\text{Re}\left(\lambda_s^i\right)$, and P represents the projection onto the linear stable subspace of the origin. Now, $\mathbb{I}$ represents the $n \times n$ identity, and so $\mathbb{I} - P$ is the complementary space associated with P, and thus the second equation in (A4) indicates that there is exponential decay in backwards time t in this direction. Once again, if $B(t) = J$, this means that $\alpha_2 = \text{Re}\left(\lambda_u^i\right)$. Thus, in the steady case the two equations in (A4) represent the exponential decays associated with the stable and unstable manifolds. The conditions (A4), therefore, provide an intuitively pleasing method to extend such hyperbolicity to unsteady flows.

APPENDIX B: ESTABLISHING HYPERBOLICITY OF (11)

It was claimed in Sec. II that (11) is a hyperbolic trajectory of the complicated unsteady flow (10). To check this, the matrix $B(t)$ associated with the linearised system in the form (A3) needs to be formed by finding the spatial derivative of $\mathbf{u}(\mathbf{x}, t)$ in (10), and then evaluating at $(\mathbf{x}^*(t), t)$. So from (10),

$$\begin{aligned} D\mathbf{u}\,(\mathbf{x}, t) = {} & D\dot{\mathbf{Q}}_t\left(\mathbf{Q}_t^{-1}(\mathbf{x})\right) D\mathbf{Q}_t^{-1}(\mathbf{x}) + D^2\mathbf{Q}_t\left(\mathbf{Q}_t^{-1}(\mathbf{x})\right) D\mathbf{Q}_t^{-1}(\mathbf{x})\, \mathbf{u}_0\left(\mathbf{Q}_t^{-1}(\mathbf{x})\right) \\ & + D\mathbf{Q}_t\left(\mathbf{Q}_t^{-1}(\mathbf{x})\right) D\mathbf{u}_0\left(\mathbf{Q}_t^{-1}(\mathbf{x})\right) D\mathbf{Q}_t^{-1}(\mathbf{x}), \end{aligned}$$

in which $D^2\mathbf{Q}_t$ is the $n \times n \times n$ tensor second-derivative of $\mathbf{g}$ and $D\mathbf{Q}_t^{-1}$ is the $n \times n$ spatial derivative of $\mathbf{Q}_t^{-1}$. By evaluating at $\mathbf{x}^*(t)$ as given in (11),

$$\begin{aligned} D\mathbf{u}\left(\mathbf{x}^*(t), t\right) &= D\dot{\mathbf{Q}}_t\left(\mathbf{m}^*\right) D\mathbf{Q}_t^{-1}\left(\mathbf{Q}_t\left(\mathbf{m}^*\right)\right) + D\mathbf{Q}_t\left(\mathbf{m}^*\right) D\mathbf{u}_0\left(\mathbf{m}^*\right) D\mathbf{Q}_t^{-1}\left(\mathbf{Q}_t\left(\mathbf{m}^*\right)\right) \\ &= D\dot{\mathbf{Q}}_t\left(\mathbf{m}^*\right) G^-(t) + G^+(t)\, J\, G^-(t) \end{aligned}$$

since $\mathbf{u}_0(\mathbf{m}^*) = \mathbf{0}$, and by using the definitions (2) and (4). The variational equation $\dot{\mathbf{w}} = D\mathbf{u}\,(\mathbf{x}^*(t), t)\,\mathbf{w}$ becomes

$$\dot{\mathbf{w}} = \left[D\dot{\mathbf{Q}}_t\left(\mathbf{m}^*\right) G^-(t) + G^+(t)\, J\, G^-(t)\right]\mathbf{w}. \tag{B1}$$

Exponential dichotomy conditions are not immediately obvious for (B1). However, define

$$\mathbf{z}(t) = G^-(t)\mathbf{w}(t), \tag{B2}$$

and hence $\mathbf{w}(t) = G^+(t)\mathbf{z}(t)$. Thus $\dot{\mathbf{w}} = D\dot{\mathbf{Q}}_t(\mathbf{m}^*) + G^+(t)\dot{z}$, enabling (B1) to be written in terms of the $\mathbf{z}$ variable as

$$\dot{\mathbf{z}} = J\,\mathbf{z}. \tag{B3}$$

By virtue of the matrix coefficient being time-independent and the hyperbolicity condition imposed in Sec. II, (B3) possesses an exponential dichotomy. Hence there exist a projection P and positive constants K_i, α_i such that (A4) is satisfied with a fundamental matrix Z of (B3) replacing Y. Let W be a fundamental matrix associated with (B1), which can then be related to Z through $Z(t) = G^-(t)W(t)$. Substituting into the first inequality in (A4) leads to the condition

$$\left\|G^-(t)W(t)PW^{-1}(s)G^+(s)\right\| \leq K_1 e^{-\alpha_1(t-s)} \text{for} t \geq s.$$

In order to establish the first exponential dichotomy condition for W, consider for $t \geq s$,

$$\begin{aligned}
\left\|W(t)PW^{-1}(s)\right\| &= \left\|G^+(t)\,G^-(t)W(t)PW^{-1}(s)G^+(s)G^-(s)\right\| \\
&= \left\|G^+(t)\,\left(G^-(t)W(t)PW^{-1}(s)G^+(s)\right)\,G^-(s)\right\| \\
&\leq \left\|G^+(t)\right\|\,\left\|G^-(t)W(t)PW^{-1}(s)G^+(s)\right\|\,\left\|G^-(s)\right\| \\
&\leq C_1 e^{-\beta t}\,K_1 e^{-\alpha_1(t-s)}\,C_2 e^{\beta s} \\
&= C_1C_2K_1\,e^{-(\alpha_1+\beta)(t-s)},
\end{aligned} \tag{B4}$$

in which the first inequality is using the standard sub-multiplicative property of matrix norms,[94] and the second is using the norm-bound conditions (6). Now, $-\alpha_1$ is the decay rate associated with the stable manifold of (B3); that is, $-\alpha_1 = \text{Re}\left(\lambda_s^i\right)$. By the condition on β given in (5), $\gamma_1 = \alpha_1 + \beta > 0$. Thus, by defining $L_1 = C_1C_2K_1$ the condition

$$\left\|W(t)PW^{-1}(s)\right\| \leq L_1 e^{-\gamma_1(t-s)} \text{ for } t \geq s \tag{B5}$$

emerges. Next, the second exponential dichotomy condition in (A4) is tackled by assuming that $s \geq t$. Following a similar argument to (B4),

$$\left\|W(t)\,(\mathbb{I} - P)\,W^{-1}(s)\right\| \leq C_1C_2K_2\,e^{-(\alpha_2-\beta)(s-t)}. \tag{B6}$$

Now define $L_2 = C_1C_2K_2$ and $\gamma_2 = \alpha_2 - \beta$, and note from (5) that $\gamma_2 = \text{Re}\left(\lambda_u^i\right) - \beta > 0$. Therefore,

$$\left\|W(t)\,(\mathbb{I} - P)\,W^{-1}(s)\right\| \leq L_2 e^{-\gamma_2(s-t)} \text{ for } s \geq t, \tag{B7}$$

which is the second exponential dichotomy condition. Since exponential dichotomy conditions have been established for Eq. (B1), $\mathbf{x}^*$ as given in (11) is a hyperbolic trajectory of (10).

APPENDIX C: LENGTHY EQUATIONS ASSOCIATED WITH THE 3D EXAMPLES

This appendix collects together equations which, because of their length, have been extracted from the main text.

1. Steady Hill's spherical vortex

Trajectories of the no-swirl version of Hill's spherical vortex obey

$$\left.\begin{aligned}
\dot{x} &= \frac{3Uc^3xz}{\left(x^2+y^2+z^2\right)^{5/2}} \\
\dot{y} &= \frac{3Uc^3yz}{\left(x^2+y^2+z^2\right)^{5/2}} \\
\dot{z} &= \frac{Uc^3}{2\left(x^2+y^2+z^2\right)^{5/2}}\left(2z^2-x^2-y^2\right) - U
\end{aligned}\right\} \tag{C1}$$

for $x^2+y^2+z^2 \geq c^2$, and

$$\left.\begin{aligned} \dot{x} &= \frac{3Uxz}{2c^2} \\ \dot{y} &= \frac{3Uyz}{2c^2} \\ \dot{z} &= \frac{3U}{2} - \frac{3U}{2c^2}\left[z^2 + 2\left(x^2+y^2\right)\right] \end{aligned}\right\} \tag{C2}$$

for $x^2+y^2+z^2 < c^2$.

2. Hill's spherical vortex modified according to (32)

Define the quantity

$$h_1(x,y,z,t) = \left(\frac{z - \frac{2c^2}{\sqrt{c^2+U^2t^2}}}{21}\right)^2 + \left(\frac{x+2y-c\cos\frac{Ut}{c} - 6c\sin\frac{Ut}{c\sqrt{2}}}{5\left(\cos\frac{Ut}{c}-3\right)\left(\cos\frac{4Ut}{c}-3\right)}\right)^2 + \left(\frac{4x-7y+21c\sin\frac{Ut}{c\sqrt{2}} + \cos\frac{Ut}{c}\left[5y-4c-15c\sin\frac{Ut}{c\sqrt{2}}\right]}{5\left(\cos\frac{Ut}{c}-3\right)\left(2+\sin\frac{Ut}{c}\right)}\right)^2.$$

The unsteady flow is now defined as follows. If $h_1(x,y,z,t) \geq c^2$, the flow obeys

$$\left.\begin{aligned}
\dot{x} &= \frac{Uc^3\left(\frac{2c^2}{\sqrt{c^2+U^2t^2}} - z\right)\left(7-5\cos\frac{Ut}{c}\right)\left(x+2y-c\cos\frac{Ut}{c}-6c\sin\frac{Ut}{c\sqrt{2}}\right)}{35\left(3-\cos\frac{Ut}{c}\right)h_1(x,y,z,t)^{5/2}} \\
&\quad + \frac{2Uc^3\left(\frac{2c^2}{\sqrt{c^2+U^2t^2}} - z\right)\left(4x-7y+21c\sin\frac{Ut}{c\sqrt{2}} + \cos\frac{Ut}{c}\left[5y-4c-15c\sin\frac{Ut}{c\sqrt{2}}\right]\right)}{35\left(3-\cos\frac{Ut}{c}\right)h_1(x,y,z,t)^{5/2}} - U\sin\frac{Ut}{c} \\
&\quad + \frac{U\left[5\left(\cos\frac{4Ut}{c}-3\right)\sin\frac{Ut}{c} + 4\left(5\cos\frac{Ut}{c}-7\right)\sin\frac{4Ut}{c}\right]\left[c\cos\frac{Ut}{c} + 6c\sin\frac{Ut}{c\sqrt{2}} - x - 2y\right]}{5c\left(\cos\frac{Ut}{c}-3\right)\left(\cos\frac{4Ut}{c}-3\right)} \\
&\quad + \frac{2U\cos\frac{Ut}{c}\left(7y-4x-21c\sin\frac{Ut}{c\sqrt{2}} + \cos\frac{Ut}{c}\left[4c-5y+15c\sin\frac{Ut}{c\sqrt{2}}\right]\right)}{5c\left(\cos\frac{Ut}{c}-3\right)\left(\sin\frac{Ut}{c}+2\right)} \\
\dot{y} &= \frac{4Uc^3\left(\frac{2c^2}{\sqrt{c^2+U^2t^2}} - z\right)\left(x+2y-c\cos\frac{Ut}{c}-6c\sin\frac{Ut}{c\sqrt{2}}\right)}{35\left(3-\cos\frac{Ut}{c}\right)h_1(x,y,z,t)^{5/2}} \\
&\quad - \frac{Uc^3\left(\frac{2c^2}{\sqrt{c^2+U^2t^2}} - z\right)\left(4x-7y+21c\sin\frac{Ut}{c\sqrt{2}} + \cos\frac{Ut}{c}\left[5y-4c-15c\sin\frac{Ut}{c\sqrt{2}}\right]\right)}{35\left(3-\cos\frac{Ut}{c}\right)h_1(x,y,z,t)^{5/2}} + \frac{3U}{\sqrt{2}}\cos\frac{Ut}{c\sqrt{2}} \\
&\quad + \frac{16U\sin\frac{4Ut}{c}\left(x+2y-c\cos\frac{Ut}{c}-6c\sin\frac{Ut}{c\sqrt{2}}\right)}{5c\left(\cos\frac{Ut}{c}-3\right)\left(\cos\frac{4Ut}{c}-3\right)} \\
&\quad + \frac{U\cos\frac{Ut}{c}\left(4x-7y+21c\sin\frac{Ut}{c\sqrt{2}} + \cos\frac{Ut}{c}\left[5y-4c-15c\sin\frac{Ut}{c\sqrt{2}}\right]\right)}{5c\left(\cos\frac{Ut}{c}-3\right)\left(\sin\frac{Ut}{c}+2\right)} \\
\dot{z} &= 21U - \frac{2c^2U^2t}{\left(c^2+U^2t^2\right)^{3/2}} \\
&\quad + \frac{21c^3U\left[2\left(\frac{\frac{2c^2}{\sqrt{c^2+U^2t^2}}-z}{21}\right)^2 - \left(\frac{x+2y-c\cos\frac{Ut}{c}-6c\sin\frac{Ut}{c\sqrt{2}}}{5\left(\cos\frac{Ut}{c}-3\right)\left(\cos\frac{4Ut}{c}-3\right)}\right)^2 - \left(\frac{4x-7y+21c\sin\frac{Ut}{c\sqrt{2}}+\cos\frac{Ut}{c}\left[5y-4c-15c\sin\frac{Ut}{c\sqrt{2}}\right]}{5\left(\cos\frac{Ut}{c}-3\right)\left(\sin\frac{Ut}{c}+2\right)}\right)^2\right]}{2h_1(x,y,z,t)^{5/2}}
\end{aligned}\right\}, \tag{C3}$$

while if $h_1(x, y, z, t) < c^2$ it is given by

$$\left.\begin{aligned}
\dot{x} &= \frac{U\left(c^2 z - 2c^2\sqrt{c^2+U^2t^2} + U^2 z t^2\right)\left(5\cos\frac{Ut}{c} - 7\right)\left(6c\sin\frac{Ut}{c\sqrt{2}} + c\cos\frac{Ut}{c} - x - 2y\right)}{70c^2\left(c^2+U^2t^2\right)\left(\cos\frac{Ut}{c} - 3\right)} \\
&\quad - \frac{U\left(\frac{2c^2}{\sqrt{c^2+U^2t^2}} - z\right)\left(4x - 7y + 21c\sin\frac{Ut}{c\sqrt{2}} + \cos\frac{Ut}{c}\left[5y - 4c - 15c\sin\frac{Ut}{c\sqrt{2}}\right]\right)}{35c^2\left(\cos\frac{Ut}{c} - 3\right)} \\
&\quad + \frac{U\left(30\sin\frac{Ut}{c} - 15\sin\frac{3Ut}{c} + 56\sin\frac{4Ut}{c} - 25\sin\frac{5Ut}{c}\right)\left(x + 2y - c\cos\frac{Ut}{c} - 6c\sin\frac{Ut}{c\sqrt{2}}\right)}{10c\left(\cos\frac{Ut}{c} - 3\right)\left(\cos\frac{4Ut}{c} - 3\right)} \\
&\quad + \frac{2U\cos\frac{Ut}{c}\left(7y - 4x - 21c\sin\frac{Ut}{c\sqrt{2}} + \cos\frac{Ut}{c}\left[4c - 5y + 15c\sin\frac{Ut}{c\sqrt{2}}\right]\right)}{5c\left(\cos\frac{Ut}{c} - 3\right)\left(\sin\frac{Ut}{c} + 2\right)} - U\sin\frac{Ut}{c} \\
\dot{y} &= \frac{2U\left(-c^2 z + 2c^2\sqrt{c^2-U^2t^2} - U^2 z t^2\right)\left(6c\sin\frac{Ut}{c\sqrt{2}} + c\cos\frac{Ut}{c} - x - 2y\right)}{35c^2\left(c^2+U^2t^2\right)\left(\cos\frac{Ut}{c} - 3\right)} \\
&\quad + \frac{U\left(\frac{2c^2}{\sqrt{c^2+U^2t^2}} - z\right)\left(4x - 7y + 21c\sin\frac{Ut}{c\sqrt{2}} + \cos\frac{Ut}{c}\left[5y - 4c - 15c\sin\frac{Ut}{c\sqrt{2}}\right]\right)}{70c^2\left(\cos\frac{Ut}{c} - 3\right)} \\
&\quad + \frac{16U\sin\frac{4Ut}{c}\left(x + 2y - c\cos\frac{Ut}{c} - 6c\sin\frac{Ut}{c\sqrt{2}}\right)}{5c\left(\cos\frac{Ut}{c} - 3\right)\left(\cos\frac{4Ut}{c} - 3\right)} \\
&\quad + \frac{U\cos\frac{Ut}{c}\left(4x - 7y + 21c\sin\frac{Ut}{c\sqrt{2}} + \cos\frac{Ut}{c}\left[5y - 4c - 15c\sin\frac{Ut}{c\sqrt{2}}\right]\right)}{5c\left(\cos\frac{Ut}{c} - 3\right)\left(\sin\frac{Ut}{c} + 2\right)} + \frac{3U}{\sqrt{2}}\cos\frac{Ut}{c\sqrt{2}} \\
\dot{z} &= -\frac{63U}{2} - \frac{2c^2U^2t}{\left(c^2+U^2t^2\right)^{3/2}} \\
&\quad + \frac{63U}{2c^2}\left[\left(\frac{z - \frac{2c^2}{\sqrt{c^2+U^2t^2}}}{21}\right)^2 + 2\left(\frac{x + 2y - c\cos\frac{Ut}{c} - 6c\sin\frac{Ut}{c\sqrt{2}}}{5\left(\cos\frac{Ut}{c} - 3\right)\left(\cos\frac{4Ut}{c} - 3\right)}\right)^2\right] \\
&\quad + \frac{63U}{2c^2}\left[2\left(\frac{4x - 7y + 21c\sin\frac{Ut}{c\sqrt{2}} + \cos\frac{Ut}{c}\left[5y - 4c - 15c\sin\frac{Ut}{c\sqrt{2}}\right]}{5\left(\cos\frac{Ut}{c} - 3\right)\left(2 + \sin\frac{Ut}{c}\right)}\right)^2\right]
\end{aligned}\right\}. \tag{C4}$$

3. Hill's spherical vortex modified according to (37)

The inverse of transformation (37) is given by

$$\mathbf{Q}_t^{-1}(\mathbf{x}) = \begin{pmatrix} c\left(\left[\dfrac{xe^{-\mu t}}{\ln z - 3 - \mu t}\right]^{1/3} - 3\right) \\ 4c\tan\dfrac{ye^{-\mu t}}{2+\cos\omega t} \\ c\ln\left(ze^{-\mu t}\right). \end{pmatrix}. \tag{C5}$$

By explicit computation from (37),

$$\det D\mathbf{Q}_t(\mathbf{x}) = -\frac{12e^{3\mu t}e^{z/c}(3c+x)^2(3c-z)(2+\cos\omega t)}{c^4\left(16c^2+y^2\right)}. \tag{C6}$$

Now, this needs to be nonzero in $\mathbf{Q}t^{-1}(\mathbf{x})$, which can be ensured by insisting on $\mathbf{Q}_t^{-1}(\mathbf{x})$ lying within the sphere of radius $2c$, for example. Expressing this condition in terms of the inverse transformation (C5) results in the domain restriction as given in (38).

The matrix norms of the relevant G matrices are explicitly computable using (9), leading to the claim (39). They are

$$\left\|G_n^+(t)\right\| = \frac{1}{c^2}e^{2\mu t}\frac{3645+e^2+\sqrt{13286025-4374e^2+e^4}}{2} \approx 3646.48\,\frac{1}{c^2}\,e^{2\mu t}\,,$$

$$\left\|G_s^+(t)\right\| = \frac{1}{c^2}e^{2\mu t}\frac{1+12393e^2+\sqrt{1-21870e^2+153586449e^4}}{2e^2} \approx 12393\,\frac{1}{c^2}\,e^{2\mu t}\,,$$

$$\left\|G_n^-(t)\right\| = c^2e^{-2\mu t}\,\frac{16}{(2+\cos\omega t)^2} \le 16\,c^2\,e^{-2\mu t}\,,$$

$$\left\|G_s^-(t)\right\| = c^2e^{-2\mu t}\,\frac{16}{(2+\cos\omega t)^2} \le 16\,c^2\,e^{-2\mu t}.$$

In order to express the unsteady flow, define the quantity

$$h(x,\,y,\,z,\,t) := \left[\left(\frac{xe^{-\mu t}}{\ln z-3-t\mu}\right)^{1/3}-3\right]^2+(\ln z-\mu t)^2+16\tan^2\frac{ye^{-\mu t}}{2+\cos\omega t}. \tag{C7}$$

Thus, the domain constraint (38) is simply stated as $h(x,\,y,\,z,\,t)<4$, and the two-dimensional manifold (43) given by $h(x,\,y,\,z,\,t)=1$. For $h(x,\,y,\,z,\,t)\ge 1$, the unsteady velocity is given by

$$\left.\begin{aligned}
\dot{x} &= \frac{Ux}{c\,(t\mu+3-\ln z)}-\frac{Up(x,\,y,\,z,\,t)}{2c\,(t\mu+3-\ln z)\,h(x,\,y,\,z,\,t)^{5/2}}-\frac{9U\,(t\mu-\ln z)\left(1+3\left[\frac{t\mu+3-\ln z}{xe^{-\mu t}}\right]^{1/3}\right)}{c\,h(x,\,y,\,z,\,t)^{5/2}}+\mu x\\
\dot{y} &= \frac{3Ue^{\mu t}\,(2+\cos\omega t)\,(\ln z-\mu t)\sin\frac{2ye^{-\mu t}}{2+\cos\omega t}}{2\,c\,h(x,\,y,\,z,\,t)^{5/2}}-\frac{\omega y\sin\omega t}{2+\cos\omega t}+\mu y\\
\dot{z} &= -\frac{U}{c}\left(\frac{\left[\left(\frac{xe^{-\mu t}}{\ln z-3-t\mu}\right)^{1/3}-3\right]^2-2\,(\ln z-\mu t)^2+16\tan^2\frac{ye^{-\mu t}}{2+\cos\omega t}}{2h(x,\,y,\,z,\,t)^{5/2}}+1\right)+\mu z
\end{aligned}\right\}, \tag{C8}$$

and for $h(x,\,y,\,z,\,t)<1$, it is

$$\left.\begin{aligned}
\dot{x} &= x\left(2c\mu+U\left(\frac{78}{t\mu+3-\ln z}-6\mu t-9\right)+6U\ln z\right)+\frac{36Ux^{4/3}e^{-\mu t/3}}{(t\mu+3-\ln z)^{4/3}}+\frac{96Ux\tan^2\frac{ye^{-\mu t}}{2+\cos\omega t}}{t\mu+3-\ln z}\\
&\quad+\frac{6Ux^{5/3}e^{-2\mu t/3}}{(t\mu+3-\ln z)^{5/3}}+27Ux^{2/3}\,(t\mu+3-\ln z)^{1/3}\,(\ln z-t\mu)\,e^{\mu t/3}\\
\dot{y} &= \frac{e^{\mu t}}{4c}\left(\frac{4cye^{-\mu t}\,(\mu\cos\omega t-\omega\sin\omega t+2\mu)}{2+\cos\omega t}+3U\,(2+\cos\omega t)\,(\ln z-\mu t)\sin\frac{2ye^{-\mu t}}{2+\cos\omega t}\right)\\
\dot{z} &= \frac{3Uz}{2c}\left(1-[\ln z-\mu t]^2-32\tan^2\frac{ye^{-\mu t}}{2+\cos\omega t}-2\left[\left(\frac{xe^{-\mu t}}{\ln z-3-t\mu}\right)^{1/3}-3\right]^2\right)+\mu z
\end{aligned}\right\}. \tag{C9}$$

[1] F. J. Beron-Vera, M. J. Olascoaga, M. G. Brown, H. Kocak, and I. Rypina, "Invariant-tori-like Lagrangian coherent structures in geophysical flows," Chaos **20**, 017514 (2010).
[2] T. Sapsis, G. Peng, and G. Haller, "Instabilities on prey dynamics in jellyfish feeding," Bull. Math. Biol. **73**, 1841–1856 (2011).
[3] R. Pierrehumbert and H. Yang, "Global chaotic mixing in isentropic surfaces," J. Atmos. Sci. **50**, 2462–2480 (1993).
[4] B. Joseph and B. Legras, "Relation between kinematic boundaries, stirring and barriers for the Antarctic polar vortex," J. Atmos. Sci. **59**, 1198–1212 (2002).

[5] M. Branicki, A. M. Mancho, and S. Wiggins, "A Lagrangian description of transport associated with front-eddy interaction: application to data from the North-Western Mediterranean Sea," Physica D **240**, 282–304 (2011).
[6] W. Tang, P. W. Chan, and G. Haller, "Lagrangian coherent structure analysis of terminal winds detected by Lidar. Part I: Turbulence structures," J. Appl. Meteorol. Climatol. **50**, 325–338 (2011).
[7] W. Tang, P. W. Chan, and G. Haller, "Lagrangian coherent structure analysis of terminal winds detected by Lidar. Part II: Structure evolution and comparison with flight data," J. Appl. Meteorol. Climatol. **50**, 2167–2183 (2011).
[8] F. Lekien, C. Coulliette, A. J. Mariano, E. H. Ryan, L. K. Shay, G. Haller, and J. Marsden, "Pollution release tied to invariant manifolds: A case study for the coast of Florida," Physica D **210**, 1–20 (2005).
[9] S. Shadden, F. Lekien, J. D. Paduan, F. P. Chavez, and J. E. Marsden, "The correlation between surface drifters and coherent structures based on high-frequency radar data in Monterey Bay," Deep-Sea Res., Part II **56**, 161–172 (2009).
[10] M. F. M. Speetjens, H. N. L. de Wispelaere, and A. A. van Steenhoven, "Multi-functional Lagrangian flow structures in three-dimensional ac electro-osmotic micro-flows," Fluid Dyn. Res. **43**, 035503 (2011).
[11] S. Balasuriya, "Optimal frequency for microfluidic mixing across a fluid interface," Phys. Rev. Lett. **105**, 064501 (2010).
[12] S. Balasuriya, "An approach for maximizing chaotic mixing in microfluidic devices," Phys. Fluids **17**, 118103 (2005).
[13] S. Balasuriya and M. D. Finn, "Energy constrained transport maximization across a fluid interface," Phys. Rev. Lett. **108**, 244503 (2012).
[14] V. Rom-Kedar, A. Leonard, and S. Wiggins, "An analytical study of transport, mixing and chaos in an unsteady vortical flow," J. Fluid Mech. **214**, 347–394 (1990).
[15] K. R. Meyer and G. R. Sell, "Melnikov transforms, Bernoulli bundles, and almost periodic perturbations," Trans. Am. Math. Soc. **314**, 63–105 (1989).
[16] K. J. Palmer, "Exponential dichotomies and transversal homoclinic points," J. Differ. Equations **55**, 225–256 (1984).
[17] S. Balasuriya, "A tangential displacement theory for locating perturbed saddles and their manifolds," SIAM J. Appl. Dyn. Syst. **10**, 1100–1126 (2011).
[18] S. Balasuriya, "Cross-separatrix flux in time-aperiodic and time-impulsive flows," Nonlinearity **19**, 2775–2795 (2006).
[19] K. Yagasaki, "Invariant manifolds and control of hyperbolic trajectories on infinite- or finite-time intervals," Dyn. Syst. **23**, 309–331 (2008).
[20] G. Haller, "Distinguished material surfaces and coherent structures in three-dimensional fluid flows," Physica D **149**, 248–277 (2001).
[21] Z. Pouransari, M. F. M. Speetjens, and H. J. H. Clercx, "Formation of coherent structures by fluid inertia in three-dimensional laminar flows," J. Fluid Mech. **654**, 5–34 (2010).
[22] M. Branicki and S. Wiggins, "An adaptive method for computing invariant manifolds in non-autonomous, three-dimensional dynamical systems," Physica D **238**, 1625–1657 (2009).
[23] S. Balasuriya, I. Mezić, and C. K. R. T. Jones, "Weak finite-time Melnikov theory and 3D viscous perturbations of Euler flows," Physica D **176**, 82–106 (2003).
[24] C. Lu, R. Gong, and J. Luo, "Analysis of stagnation points for a pumping well in recharge areas," J. Hydrol. **373**, 442–452 (2009).
[25] O. A. van Herwaarden, "Spread of pollutant by dispersive groundwater flow," SIAM J. Appl. Math. **54**, 26–41 (1994).
[26] P. H. Gaskell, M. D. Savage, and H. M. Thompson, "Stagnation-saddle points and flow patterns in Stokes flow between contra-rotating cylinder," J. Fluid Mech. **370**, 221–247 (1998).
[27] F. Arai, A. Ichikawa, T. Fukuda, K. Horio, and K. Itoigawa, "Stagnation point control by pressure balancing in microchannel for high speed and high purity separation of microobject," in *Proceedings of the 2001 IEEE/RSJ International Conference on Intelligent Robots and Systems*, Maui, Hawaii, USA, 29 Oct.–3 Nov, 2001 (IEEE, 2001), Vol. 3, pp. 1343–1348.
[28] B. J. Bentley and L. G. Leal, "A computer-controlled four-roll mill for investigations of particle and drop dynamics in two-dimensional shear flows," J. Fluid Mech. **167**, 219–240 (1986).
[29] W. Xu and S. J. Muller, "Exploring both sequence detection and restriction endonuclease cleavage kinetics by recognition site via single-molecule microfluidic trapping," Lab Chip **11**, 435–442 (2011).
[30] J. Soulages, M. S. N. Oliveira, P. C. Souza, M. A. Alves, and G. H. McKinley, "Investigating the stability of viscoelastic stagnation flows in T-shaped microchannels," J. Non-Newtonian Fluid Mech. **163**, 9–24 (2009).
[31] S. Hu, D. E. LaCroix, and A. R. McFarland, "Stagnation point displacement: control of losses on a conically shaped aerosol distributor," Aerosol Sci. Technol. **43**, 311–321 (2009).
[32] J. A. Whitehead, "Topographic control of oceanic flows in deep passages and straits," Rev. Geophys. **36**, 423–440, doi:10.1029/98RG01014 (1998).
[33] S. Balasuriya, "Gradient evolution for potential vorticity flows," Nonlinear Processes Geophys. **8**, 253–263 (2001).
[34] R. Pierrehumbert, "Chaotic mixing of tracer and vorticity by modulated travelling Rossby waves," Geophys. Astrophys. Fluid Dyn. **58**, 285–319 (1991).
[35] D. del Castillo Negrete and P. J. Morrison, "Chaotic transport by Rossby waves in shear flow," Phys. Fluids A **5**, 948–965 (1993).
[36] I. I. Rypina, M. G. Brown, and H. Koçak, "Transport in an idealized three-gyre system with applications to the Adriatic Sea," J. Phys. Oceanogr. **39**, 675–690 (2009).
[37] G. Haller, "Finding finite-time invariant manifolds in two-dimensional velocity fields," Chaos **10**, 99–108 (2000).
[38] G. Haller and A. C. Poje, "Finite time transport in aperiodic flows," Physica D **119**, 352–380 (1998).
[39] W. A. Coppel, *Dichotomies in Stability Theory*, Lecture Notes in Mathematics Vol. 629 (Springer-Verlag, Berlin, 1978).
[40] F. Battelli and C. Lazzari, "Exponential dichotomies, heteroclinic orbits and Melnikov functions," J. Differ. Equations **86**, 342–366 (1986).
[41] B. Krauskopf, H. M. Osinga, E. J. Doedel, M. E. Henderson, J. Guckenheimer, A. Vladimirsky, M. Dellnitz, and O. Junge, "A survey of method's for computing (un)stable manifold of vector fields," Int. J. Bifurcation Chaos **15**, 763–791 (2005).
[42] G. Haller and G.-C. Yuan, "Lagrangian coherent structures and mixing in two-dimensional turbulence," Physica D **147**, 352–370 (2000).

[43] T. Peacock and J. Dabiri, "Introduction to focus issue: Lagrangian coherent structures," Chaos **20**, 017501 (2010).
[44] G. Boffetta, G. Lacorata, G. Radaelli, and A. Vulpiani, "Detecting barriers to transport: a review of different techniques," Physica D **159**, 58–70 (2001).
[45] A. Provenzale, "Transport by coherent barotropic vortices," Annu. Rev. Fluid Mech. **31**, 55–93 (1999).
[46] J. Kasten, C. Petz, I. Hotz, H.-C. Hege, B. R. Noack, and G. Tadmor, "Lagrangian feature extraction of the cylinder wake," Phys. Fluids **22**, 091108 (2010).
[47] A. de la Camara, C. R. Mechoso, K. Ide, R. Walterscheid, and G. Schubert, "Polar night vortex breakdown and large-scale stirring in the southern stratosphere," Clim. Dyn. **35**, 965–975 (2010).
[48] K. Katija, W. T. Beaulieu, C. Regula, S. P. Colin, J. H. Costello, and J. O. Dabiri, "Quantification of flows generated by the hydromedusa Aequorea victoria: a Lagrangian coherent structure analysis," Mar. Ecol.: Prog. Ser. **435**, 111–123 (2011).
[49] O. Titaud, J. M. Brankart, and J. Verron, "On the use of finite-time Lyapunov exponents and vectors for direct assimilation of tracer images into ocean models," Tellus Series A: Dynamics Meteorology and Oceanography **63**, 1038–1051 (2011).
[50] D. Borgogno, D. Grasso, F. Pegoraro, and T. J. Schep, "Barriers in the transition to global chaos in collisionless magnetic reconnection. I. Ridges of the finite time Lyapunov exponent field," Phys. Plasmas **18**, 102307 (2011).
[51] S. C. Shadden, F. Lekien, and J. E. Marsden, "Definition and properties of Lagrangian coherent structures from finite-time Lyapunov exponents in two-dimensional aperiodic flows," Physica D **212**, 271–304 (2005).
[52] S. L. Brunton and C. W. Rowley, "Fast computation of finite-time Lyapunov exponent fields for unsteady flows," Chaos **20**, 017503 (2010).
[53] D. Lipinski and K. Mohseni, "A ridge tracking algorithm and error estimate for efficient computation of Lagrangian coherent structures," Chaos **20**, 017504 (2010).
[54] C. Senatore and S. D. Ross, "Detection and characterization of transport barriers in complex flows via ridge extraction of the finite time Lyapunov exponent field," Int. J. Numer. Methods Eng. **86**, 1163–1174 (2011).
[55] G. Haller, "A variational theory for Lagrangian coherent structures," Physica D **240**, 574–598 (2011).
[56] M. Farazmand and G. Haller, "Erratum and addendum to "A variational theory for Lagrangian coherent structures"," Physica D **241**, 439–441 (2012).
[57] M. Farazmand and G. Haller, "Computing Lagrangian coherent structures from variational LCS theory," Chaos **22**, 013128 (2012).
[58] G. Haller, "Lagrangian coherent structures from approximate velocity data," Phys. Fluids A **14**, 1851–1861 (2002).
[59] G. Haller and T. Sapsis, "Lagrangian coherent structures and the smallest finite-time Lyapunov exponent," Chaos **21**, 023115 (2011).
[60] I. Mezić, S. Loire, V. A. Fonoberov, and P. Hogan, "A new mixing diagnostic and Gulf oil spill movement," Science **330**, 486–489 (2010).
[61] Z. Levnajić and I. Mezić, "Ergodic theory and visualization. I. Mesochronic plots for visualization of ergodic partition and invariant sets," Chaos **20**, 033114 (2010).
[62] C. Mendoza and A. Mancho, "Hidden geometry of ocean flows," Phys. Rev. Lett. **105**, 038501 (2010).
[63] J. A. J. Jimenez-Madrid and A. M. Mancho, "Distinguished trajectories in time dependent vector fields," Chaos **19**, 013111 (2009).
[64] A. M. Mancho, E. Hernández-García, D. Small, S. Wiggins, and V. Fernández, "Lagrangian transport through an ocean front in the northwestern Mediterranean Sea," J. Phys. Oceanogr. **38**, 1222–1237 (2008).
[65] M. Dellnitz and O. Junge, "Almost invariant sets in Chua's circuit," Int. J. Bifurcation Chaos **7**, 2475–2485 (1997).
[66] I. Mezić and S. Wiggins, "A method for visualization of invariant sets of dynamical systems based on the ergodic partition," Chaos **9**, 213–218 (1999).
[67] I. Mezić and A. Banaszuk, "Comparison of systems with complex behavior," Physica D **197**, 101–133 (2004).
[68] G. Froyland and K. Padberg, "Almost-invariant sets and invariant manifolds—connecting probabilistic and geometric descriptions of coherent structures in flows," Physica D **238**, 1507–1523 (2009).
[69] G. Froyland, S. Lloyd, and N. Santitissadeekorn, "Coherent sets for nonautonomous dynamical systems," Physica D **239**, 1527–1541 (2010).
[70] G. Froyland, N. Santitissadeekorn, and A. Monahan, "Transport in time-dependent dynamical systems: finite-time coherent sets," Chaos **20**, 043116 (2010).
[71] M. R. Allshouse and J.-L. Thiffeault, "Detecting coherent structures using braids," Physica D **241**, 95–105 (2012).
[72] G. Haller and F. J. Beron-Vera, "Geodesic theory of transport barriers in two-dimensional flows," Physica D **241**, 1680–1702 (2012).
[73] G. Froyland and K. Padberg, "Finite-time entropy: a probabilistic method for measuring nonlinear stretching," Physica D **241**, 1612–1628 (2012).
[74] M. Budišić and I. Mezić, "Geometry of ergodic quotient reveals coherent structures in flows," Physica D **241**, 1255–1269 (2012).
[75] J. Guckenheimer and P. Holmes, *Nonlinear Oscillations, Dynamical Systems and Bifurcations of Vector Fields* (Springer, New York, 1983).
[76] A. R. Robinson, "Overview and summary of eddy science," in *Eddies in Marine Science*, edited by A. R. Robinson (Springer, Berlin, 1983).
[77] E. J. Hopfinger and G. J. F. van Heijst, "Vortices in rotating fluids," Annu. Rev. Fluid Mech. **25**, 241–289 (1993).
[78] M. V. Nezlin and E. N. Snezhkin, *Rossby Vortices, Spiral Structures, Solitons* (Springer, Berlin, 1993).
[79] A. Okubo, "Horizontal dispersion of floatable trajectories in the vicinity of velocity singularities such as convergencies," Deep-Sea Res. **17**, 445–454 (1970).
[80] J. Weiss, "The dynamics of enstrophy transfer in two-dimensional hydrodynamics," Physica D **48**, 273–294 (1991).
[81] H. J. Lugt, "The dilemma of defining a vortex," in *Recent Developments in Theoretical and Experimental Fluid Mechanics*, edited by U. Müller, K. G. Riesner, and B. Schmidt (Springer, Berlin, 1979), pp. 309–321.

[82] R. Cucitore, M. Quadrio, and A. Baron, "On the effectiveness and limitations of local criteria for the identification of a vortex," European Journal of Mechanics - B/Fluids **18**, 261–282 (1999).
[83] D. Elhmaïdi, A. Provenzale, and A. Babiano, "Elementary topology of two-dimensional turbulence from a Lagrangian viewpoint and single-particle dispersion," J. Fluid Mech. **257**, 533–558 (1993).
[84] M. Tabor and I. Klapper, "Stretching and alignment in chaotic and turbulent flows," Chaos, Solitons Fractals **4**, 1031–1055 (1994).
[85] G. Haller, "An objective definition of a vortex," J. Fluid Mech. **525**, 1–26 (2005).
[86] A. N. Kolmogorov, "On the conservation of conditionally periodic motions for a small change in Hamiltonians function," Dokl. Akad. Nauk SSSR **98**, 527–530 (1954).
[87] V. I. Arnold, "Proof of a theorem of A. N. Kolmogorov on the preservation of conditionally periodic motions under a small perturbation of the Hamiltonian," Russ. Math. Surveys **18**, 9–36 (1963).
[88] J. Moser, "On invariant curves of area-preserving mappings of an annulus," Nachr. Akad. Wiss. Goett. II, Math.-Phys. Kl. **II**, 1–20 (1962).
[89] H. W. Broer, G. B. Huitema, and F. Takens, "Unfolding of quasi-periodic tori," Mem. Amer. Math. Soc. **83**(421), 1–82 (1990).
[90] U. Vaidya and I. Mezić, "Existence of invariant tori in three dimensional maps with degeneracy," Physica D **241**, 1136–1145 (2012).
[91] Z. H. Xia, "Existence of invariant tori in volume-preserving diffeomorphisms," Ergod. Theory Dyn. Syst. **12**, 621–631 (1992).
[92] C. Q. Cheng and Y. Sun, "Existence of KAM tori in degenerate Hamiltonian systems," J. Differ. Equations **114**, 288–335 (1994).
[93] J. Jeong and F. Hussain, "On the identification of a vortex," J. Fluid Mech. **285**, 69–94 (1995).
[94] R. A. Horn and C. R. Johnson, *Matrix Analysis* (Cambridge University Press, Cambridge, UK, 1999).
[95] C. A. Truesdell, *A First Course in Rational Continuum Mechanics, Part I: Fundamental Concepts* (Academic, Boston, 1977).
[96] J. M. Ottino, *The Kinematics of Mixing: Stretching, Chaos, and Transport* (Cambridge University Press, Cambridge, UK, 1989).
[97] P. J. Holmes and D. Whitley, "On the attracting set for Duffing's equation," Physica D **7**, 111–123 (1983).
[98] S. Wiggins, *Chaotic Transport in Dynamical Systems* (Springer-Verlag, New York, 1992).
[99] S. Wiggins, "Chaos in the quasiperiodically forced Duffing oscillator," Phys. Lett. A **124**, 138–142 (1987).
[100] A. M. Mancho, D. Small, S. Wiggins, and K. Ide, "Computation of stable and unstable manifolds of hyperbolic trajectories in two-dimensional, aperiodically time-dependent vector fields," Physica D **182**, 188–222 (2003).
[101] D. Beigie, A. Leonard, and S. Wiggins, "Chaotic transport in the homoclinic and heteroclinic tangle regions of quasiperiodically forced two-dimensional dynamical systems," Nonlinearity **4**, 775–819 (1991).
[102] J. M. Perales and J. M. Vega, "Dynamics of nearly unstable axisymmetric liquid bridges," Phys. Fluids **23**, 012107 (2011).
[103] D. M. Slater, D. A. Lopez, A. H. Hirsa, and P. H. Steen, "Chaotic motions of a forced droplet-droplet oscillator," Phys. Fluids **20**, 092107 (2008).
[104] H. Lamb, *Hydrodynamics* (Cambridge University Press, Cambridge, 1879).
[105] V. I. Arnold, "Sur la topologie des écoulements stationnaires des fluides parfaits," C. R. Acad. Sci. Paris **261**, 17–20 (1965).
[106] J. F. Harper and D. W. Moore, "Motion of a spherical liquid drop at high Reynolds number," J. Fluid Mech. **32**, 367–391 (1968).
[107] T. S. Laker and S. M. Ghiaasiaan, "Monte-Carlo simulation of aerosol transport in rising spherical bubbles with internal circulation," J. Aerosol Sci. **35**, 473–488 (2004).
[108] M. Shusser and D. Weihs, "Compound drops as spherical shell vortices," Fluid Dyn. Res. **42**, 025502 (2010).
[109] R. Balasubramaniam and R. S. Subramanian, "The migration of a drop in a uniform temperature gradient at large Marangoni numbers," Phys. Fluids **12**, 733–743 (2000).
[110] Y. Hattori and K. Hijiya, "Short-wavelength stability analysis of Hill's vortex with/without swirl," Phys. Fluids **22**, 074104 (2010).
[111] A. Lifschitz, "Instabilities of ideal fluids and related topics," Z. Angew. Math. Mech. **75**, 411–422 (1995).
[112] T. Rozi and Y. Fukumoto, "The most unstable perturbation of wave-packet form inside Hill's vortex," J. Phys. Soc. Jpn. **69**, 2700–2701 (2000).
[113] T. Sapsis and G. Haller, "Clustering criterion for inertial particles in two-dimensional time-periodic and three-dimensional steady flows," Chaos **20**, 017515 (2010).
[114] H. E. Lomeli and R. Ramirez-Ros, "Separatrix splitting in 3D volume preserving maps," SIAM J. Appl. Dyn. Syst. **7**, 1527–1557 (2008).
[115] J. R. Angilella and J. P. Brancher, "Note on chaotic advection in an oscillating drop," Phys. Fluids **15**, 261–264 (2003).
[116] D. Robinson and D. Rockwell, "Construction of three-dimensional images of flow structure via particle tracking techniques," Exp. Fluids **14**, 257–270 (1993).
[117] B. A. Mosovsky and J. D. Meiss, "Transport in transitory dynamical systems," SIAM J. Appl. Dyn. Syst. **10**, 35–65 (2011).
[118] B. Sandstede, S. Balasuriya, C. K. R. T. Jones, and P. D. Miller, "Melnikov theory for finite-time vector fields," Nonlinearity **13**, 1357–1377 (2000).
[119] A. Berger, "On finite-time hyperbolicity," Commun. Pure Appl. Anal. **10**, 963–981 (2011).
[120] L. H. Duc and S. Siegmund, "Existence of finite-time hyperbolic trajectories for planar Hamiltonian flows," J. Dyn. Differ. Equ. **23**, 475–494 (2011).